J. Fluid Mech. (2005), *vol.* 527, *pp.* 235–264.
DOI: 10.1017/S0022112004003131 Printed in the United Kingdom

Non-conservation of 'geostrophic mass' in the presence of a long boundary and the related Kelvin wave

By G. M. REZNIK[1] AND G. G. SUTYRIN[2]

[1]P.P. Shirshov Institute of Oceanology, Moscow, Russia

[2]Graduate School of Oceanography, University of Rhode Island, Rhode Island, USA

(Received 14 November 2003 and in revised form 20 October 2004)

The evolution of a localized flow in a half-plane bounded by a rigid wall is analysed when the total mass is not conserved within the equivalent-barotropic quasi-geostrophic (QG) approximation. A simple formula expressing the total geostrophic mass in terms of the QG potential vorticity is derived and used to estimate the range of the geostrophic mass variability. The behaviour of the total mass is analysed for a system of two point vortices interacting with a wall. Distributed localized perturbations are examined by means of numerical experiments using the QG model. Two types of time variability of the total geostrophic mass are revealed: oscillating (the mass oscillates near some mean value) and limiting (the mass tends to some constant value with increasing time).

In the framework of a rotating shallow-water model, the QG model is known to describe the slow evolution of the geostrophic vorticity, assuming the Rossby number to be small. Consideration of the next-order dynamics shows that conservation of the total mass and circulation is provided by a compensating jet taking away the surplus or shortage of mass from the localized geostrophic disturbance. The along-wall jet expands with the fast speed of Kelvin waves to the right of the initial perturbation. The slow time-dependent amplitude determines the jet sign and intensity at each instant. The dynamics of the compensating jet are discussed for both oscillating and limiting regimes revealed by the QG analysis.

The role of Kelvin waves in establishing the usual Phillips condition for conservation of circulation of the along-wall QG velocity is discussed. In the case of periodic motion or motion in a finite domain, the approximation of an infinitely long boundary can be used if (i) the typical basin scale greatly exceeds the typical size of the localized perturbation and the Rossby scale; and (ii) the time does not exceed the typical time required for the Kelvin wave to travel the typical basin scale. Both these conditions are typical of synoptic variability in the ocean.

1. Introduction

This work is motivated by the fact (not well-known) that for a localized flow near an infinitely long boundary (e.g. in a channel or half-plane), the standard derivation of quasi-geostrophic (QG) equations is incomplete. In particular, it cannot provide: (i) conservation of geostrophic mass; (ii) locality of all successive approximations. The QG approximation is based on taking into account only a slow rate of evolution for fast rotating fluid (small Rossby number). In this work we elucidate that this is not adequate for domains with long boundaries (much longer than the flow scale that

is typical for synoptic variability in the ocean) and look closely at the interaction of slow and fast modes through analytical and numerical modelling.

First, we consider the standard derivation of QG equations on the semi-infinite f-plane from a full rotating shallow-water (RSW) system which is often used to reproduce the most important vertical mode of large-scale planetary flows when their vertical scale is much less than their horizontal. The non-dimensional RSW equations take the form

$$\varepsilon\frac{\partial U}{\partial T}+\varepsilon\left(U\frac{\partial U}{\partial x}+V\frac{\partial U}{\partial y}\right)-V=-\frac{\partial P}{\partial x}, \tag{1.1a}$$

$$\varepsilon\frac{\partial V}{\partial T}+\varepsilon\left(U\frac{\partial V}{\partial x}+V\frac{\partial V}{\partial y}\right)+U=-\frac{\partial P}{\partial y}, \tag{1.1b}$$

$$\varepsilon\frac{\partial \Pi}{\partial T}+\varepsilon\left\{\frac{\partial(U\Pi)}{\partial x}+\frac{\partial(V\Pi)}{\partial y}\right\}=0, \quad \Pi=\frac{\partial V}{\partial x}-\frac{\partial U}{\partial y}-P. \tag{1.1c, d}$$

Here $\boldsymbol{V}=(U(x, y, T), V(x, y, T))$ is the two-dimensional velocity field, P is the geopotential perturbation related to the dimensionless elevation as $H=H_0(1+\varepsilon P(x, y, T))$ is the layer depth, the parameter $\varepsilon=U_0/fR_d$ is the Rossby number, and U_0 is the horizontal velocity scale. The Rossby scale $R_d=\sqrt{gH_0}/f$ and the typical geostrophic time $(\varepsilon f)^{-1}$ are chosen as the spatial and time scales, respectively; g and f are the acceleration due to gravity and Coriolis parameter, respectively.

The velocity obeys the no-flux boundary condition at the rigid wall $y=0$

$$V=0 \text{ at } y=0. \tag{1.2}$$

If we assume that the motion is slow and the Rossby number ε is small, as usual, the QG solution is sought in the form of the following asymptotic expansions (see e.g. Pedlosky 1987):

$$(U, V, P)=(U_0, V_0, P_0)(x, y, T)+\varepsilon(U_1, V_1, P_1)(x, y, T)+\cdots. \tag{1.3}$$

At the lowest order we obtain from (1.1), (1.2):

$$V_0=\frac{\partial \Psi}{\partial x}, U_0=-\frac{\partial \Psi}{\partial y}, \quad \Psi=P_0, \tag{1.4a–c}$$

$$\frac{\partial(\nabla^2\Psi-\Psi)}{\partial T}+J(\Psi, \nabla^2\Psi)=0, \quad \frac{\partial \Psi}{\partial x}=0 \text{ at } y=0 \tag{1.4d, e}$$

Here $J(a, b)=\partial(a, b)/\partial(x, y)$ is the Jacobian operator. Let the initial field

$$\Psi|_{t=0}=\Psi_I(x, y) \tag{1.5}$$

be localized, i.e.

$$\Psi_I\to 0, \quad y\to+\infty, \quad x\to\pm\infty. \tag{1.6}$$

Here and below the subscript 'I' denotes initial fields.

Obviously, for conditions (1.4e), (1.6) to be consistent, it is necessary that

$$\Psi_I=0 \text{ at } y=0. \tag{1.7}$$

We assume that the decay (1.6) is sufficiently rapid so that the initial energy and enstrophy are finite.

We are looking for the solution that conserves energy and enstrophy (note that these quantities are conserved under condition (1.4e)). This means that conditions of

locality (1.6) are valid at any time, i.e.

$$\Psi \to 0, \quad y \to +\infty, \quad x \to \pm\infty, \tag{1.8}$$

since in the opposite case the energy and enstrophy become infinite. Therefore, by virtue of (1.4*e*) and (1.8), in the localized case the QG streamfunction is always identical to zero at the infinitely long boundary:

$$\Psi = 0 \text{ at } y = 0. \tag{1.9}$$

It readily follows from (1.4*d*) that the total geostrophic mass

$$\overline{M} = \int_{y>0} \Psi \,\mathrm{d}x\,\mathrm{d}y$$

is conserved only if

$$\int_{-\infty}^{\infty} \frac{\partial^2 \Psi}{\partial y \partial T}\bigg|_{y=0} \mathrm{d}x = 0. \tag{1.10}$$

But the problem (1.4*d*), (1.5), (1.9) is well-posed and, therefore, condition (1.10), generally, is not satisfied (see § 2 below and Reznik & Grimshaw 2002, hereafter referred to as RG).

The first-order velocity normal to the wall has the form

$$V_1 = \frac{\partial P_1}{\partial x} + \frac{\partial U_0}{\partial T} + U_0 \frac{\partial U_0}{\partial x} + V_0 \frac{\partial U_0}{\partial y}; \tag{1.11}$$

therefore, the first-order no-flux condition is written as

$$\frac{\partial P_1}{\partial x} = -\left(\frac{\partial U_0}{\partial T} + U_0 \frac{\partial U_0}{\partial x} \right) \text{ at } y = 0. \tag{1.12}$$

For the asymptotic procedure to be self-consistent P_1 is also required to be localized. By virtue of (1.4*b*), (1.12) this is possible only under the condition (1.10) which, generally, is not satisfied, as mentioned above. Thus, the 'slow' solution (1.3) of problem (1.1), (1.2), (1.5), (1.6) does not conserve the total mass and is not localized.

The locality of solution and mass conservation can be satisfied only in the framework of the full RSW model, taking into account the fast Kelvin waves as demonstrated in RG. It was shown that the total (geostrophic + ageostrophic) mass is conserved due to the compensating along-shore jet 'emanating' from the localized QG disturbance. This jet, formed by the first-order Kelvin wave plus the slow correction P_1, provides a sink or source of the QG mass. Note that the composite (geostrophic + ageostrophic) first-order solution is localized, although the correction P_1 and the first-order Kelvin wave are non-localized separately. The locality condition (1.8) is crucial in the above consideration since in the case of non-localized (periodic or non-periodic along the y-axis) motion, the boundary streamfunction $\Psi|_{y=0} = c(T)$ is, generally, non-zero, being determined from the no-flux condition for the ageostrophic first-order velocity field (cf. Phillips 1954; McWilliams 1977). It is important to note that the above consideration does not mean that the QG approximation is 'deficient' or breaks down in the localized case: equations (1.4), (1.5), (1.9) correctly describe the slow component of motion as demonstrated in RG. But, contrary to non-localized motion, in this case the lowest-order QG dynamics should be supplemented with the fast Kelvin wave to provide the solution locality and mass conservation.

Dorofeyev & Larichev (1992) met an analogous problem when considering the reflection of linear Rossby waves from the meridional boundary in the framework of

the RSW model on the β-plane. They revealed that the total mass of Rossby waves is not conserved, and the surplus or shortage of mass is taken away by fast Kelvin waves. Also, Helfrich & Pedlosky (1995) examined the QG motion in periodic and unbounded channels and indicated that in the localized case non-conservation of slow circulation results in radiation of Kelvin waves 'emanating from the local region' of slow motion.

The key role of the Kelvin waves in the process of geostrophic adjustment near boundaries was investigated in a number of studies after the pioneering work by Gill (1976) (e.g. Hermann, Rhines & Johnson 1989; Tomasson & Melvile 1992; Helfrich, Kuo & Pratt 1999; RG). Interaction of Kelvin waves with other modes of the system was examined, for example, by Miles (1972), Grimshaw & Allen (1988) and McCalpin (1995). In the presence of slowly varying environmental parameters, the Kelvin wave can be described by an approximate solution where along-shore geostrophy is typically retained (e.g. Fedorov & Melvile 1996; Helfrich *et al.* 1999).

The aim of this paper is to examine the variability of the total mass for the slow geostrophic flow in the localized case and the related Kelvin wave responsible for the mass conservation. The paper is organized as follows. In § 2 we derive the general formula expressing the mass of slow QG component in terms of the QG potential vorticity (PV). Using this formula we obtain limits of the QG mass variability and show that the mass variations are determined by the displacements of fluid elements with non-zero PV perpendicular to the boundary. The simplest system possessing this property consists of two point vortices interacting with each other and with the wall. The dynamics of this system are analysed in § 3. Distributed localized perturbations are examined by means of numerical experiments, described in § 4, using the QG model. Two types of time variability of the QG mass are revealed: oscillating (the mass oscillates near some mean value) and limiting (the mass tends to some constant value with increasing times). The first-order correction to the QG solution describing the compensating jet is derived in § 5 by asymptotic analysis of the full RSW model for a small Rossby number. Dynamics of the compensating jet for various regimes of QG mass variability are examined. A comparison between the localized and periodic solutions is discussed in § 6 where limits of validity of the model considered for a localized disturbance interacting with an infinitely long boundary are obtained. In § 7 our results are summarized.

2. Some general results for the QG model

2.1. *Formulae for the geostrophic mass in the presence of a boundary*

We start with the QG potential vorticity equation (1.4d) with initial and boundary conditions (1.5), (1.6), (1.9). It was demonstrated in RG (§ 4.3) that the energy and enstrophy of the localized slow motion are conserved but the total geostrophic mass

$$\overline{M} = \int_{y>0} \Psi \, \mathrm{d}x \, \mathrm{d}y \tag{2.1}$$

is not conserved. To show this we integrate (1.4d) over the half-plane $y > 0$ to obtain the equation

$$\frac{\partial \overline{M}}{\partial T} = F = -\int_{-\infty}^{\infty} \left. \frac{\partial^2 \Psi}{\partial y \partial T} \right|_{y=0} \mathrm{d}x, \tag{2.2}$$

and take into account that the lowest-order along-wall velocity circulation

$$\Gamma = -\int_{-\infty}^{\infty} \left.\frac{\partial \Psi}{\partial y}\right|_{y=0} \mathrm{d}x \tag{2.3}$$

is not a conserved quantity.

Here we express Ψ and the total geostrophic mass (2.1) in terms of the potential vorticity $Q = \nabla^2\Psi - \Psi$. To find $\overline{M}$ we integrate this equation over x:

$$\frac{\mathrm{d}^2 H}{\mathrm{d}y^2} - H = R = \int_{-\infty}^{\infty} Q\,\mathrm{d}x,\ H = \int_{-\infty}^{\infty} \Psi\,\mathrm{d}x. \tag{2.4a, b}$$

Using (1.9) we have from (2.4a):

$$H = -\frac{1}{2}\left(\mathrm{e}^{y}\int_{y}^{\infty} R\mathrm{e}^{-y}\,\mathrm{d}y + \mathrm{e}^{-y}\int_{0}^{y} R\mathrm{e}^{y}\,\mathrm{d}y\right) + \frac{1}{2}\mathrm{e}^{-y}\int_{0}^{\infty} R\mathrm{e}^{-y}\,\mathrm{d}y. \tag{2.4c}$$

Integration of (2.4a) over y gives

$$\overline{M} = -\int_{y>0} Q\,\mathrm{d}x\,\mathrm{d}y - \left.\frac{\mathrm{d}H}{\mathrm{d}y}\right|_{y=0}. \tag{2.5}$$

Substituting (2.4c) into (2.5) we arrive at the following formula for the total geostrophic mass:

$$\overline{M} = -\int_{y>0} Q(x, y, t)(1 - \mathrm{e}^{-y})\,\mathrm{d}y. \tag{2.6}$$

It is useful to represent the integral in (2.6) in terms of the Lagrangian coordinates x_0, y_0:

$$\overline{M} = -\int_{y_0>0} Q_0(x_0, y_0)\left[1 - \mathrm{e}^{-y(x_0, y_0, t)}\right]\mathrm{d}x_0\,\mathrm{d}y_0. \tag{2.7}$$

Here $Q_0(x_0, y_0)$ is the initial potential vorticity field and the Lagrangian coordinates x_0, y_0 are related to the Eulerian coordinates x, y in the following way:

$$x = x(x_0, y_0, t),\ y = y(x_0, y_0, t),\ \boldsymbol{r}|_{t=0} = (x_0, y_0), \tag{2.8}$$

$$\left.\frac{\partial x}{\partial t}\right|_{x_0, y_0} = u(x, y, t) = -\frac{\partial \Psi}{\partial y},\ \left.\frac{\partial y}{\partial t}\right|_{x_0, y_0} = v(x, y, t) = \frac{\partial \Psi}{\partial x}, \tag{2.9a, b}$$

where u, v are the geostrophic velocity components.

Representations (2.6), (2.7) allow us to draw two simple but important conclusions. First, the mass of perturbation steadily translated along the boundary $y = 0$ does not change in time, as readily seen from (2.6). Second, it follows from (2.7) that the total mass changes are determined by the displacements of fluid particles perpendicular to the boundary $y = 0$; displacements along the boundary do not influence the total mass $\overline{M}$. Note also that only the displacements of fluid particles with non-zero PV make a contribution to the integral (2.7).

Multiplying (1.4d) by y and integrating the resulting equation over the half-plane $y > 0$ we obtain the useful relationship

$$\int_{y>0} yQ(x, y, t)\,\mathrm{d}x\,\mathrm{d}y = \mathrm{const} = C_0, \tag{2.10}$$

which means that the 'PV centroid' remains at a fixed distance from the wall. In the Lagrangian variables (2.10) takes the form

$$\int_{y_0>0} y(x_0, y_0, t) Q_0(x_0, y_0)\, \mathrm{d}x_0\, \mathrm{d}y_0 = \text{const} = C_0. \tag{2.11}$$

2.2. *Limits of the geostrophic mass variability*

It readily follows from (2.6), (2.7) that the absolute value of the geostrophic mass $|\overline{M}|$ is bounded from above by the integral of the PV modulus:

$$|\overline{M}| \leqslant \int_{y>0} |Q(x, y, t)| \mathrm{d}x\, \mathrm{d}y = \int_{y_0>0} |Q_0(x_0, y_0)|\, \mathrm{d}x_0\, \mathrm{d}y_0. \tag{2.12}$$

It is possible, however, to obtain a subtler estimate for $|\overline{M}|$ in the case of sign-defined PV. In the integrand in (2.7) the initial PV Q_0 is given by the initial conditions and the total mass changes only due to the time-dependent displacements y of the fluid particles perpendicular to the wall. In turn, the displacements obey the restriction (2.11). What is the range of the total mass variability generated by the displacements y satisfying (2.11) given initial PV distribution Q_0? We emphasize that we mean all possible displacements, not only those obeying equations (2.8), (2.9) determining the Lagrangian coordinates.

To answer this question we investigate extrema of the functional

$$\overline{M}_a = -\int_{y_0>0} Q_0(x_0, y_0)\left[1 - \mathrm{e}^{-\bar{y}(x_0, y_0)}\right] \mathrm{d}x_0\, \mathrm{d}y_0 \tag{2.13a}$$

under the condition

$$\int_{y_0>0} \bar{y}(x_0, y_0) Q_0(x_0, y_0)\, \mathrm{d}x_0\, \mathrm{d}y_0 = \text{const} = C_0, \tag{2.13b}$$

assuming $Q_0(x_0, y_0)$ to be given and varying $\bar{y}(x_0, y_0)$. Simple analysis using the Lagrange multipliers method (see Appendix A) indicates that the extremal of the problem (2.13) is given by the equation

$$\bar{y} = \bar{y}_e = \frac{\displaystyle\int_{y_0>0} y_0 Q_0(x_0, y_0)\, \mathrm{d}x_0\, \mathrm{d}y_0}{\displaystyle\int_{y_0>0} Q_0(x_0, y_0)\, \mathrm{d}x_0\, \mathrm{d}y_0} \tag{2.14}$$

where $\bar{y}_e$ is a constant distance of the PV centroid from the wall.

Calculation of the second variation on the extremal (2.14) shows that the second variation is sign-defined only if the PV Q_0 does not change its sign, i.e. sufficient conditions for the existence of a maximum or minimum of the functional $\overline{M}_a$ are satisfied only in the case of PV of one sign. Also, the coordinate $\bar{y}_e$ is positive for Q_0 of a fixed sign. Thus, for PV of one sign the absolute value of functional (2.13a) is maximal on extremal (2.14), i.e. we have the following inequality:

$$|\overline{M}| \leqslant |\overline{M}_a|_{\max} = \left(1 - \mathrm{e}^{-\bar{y}_e}\right) \int_{y_0>0} |Q_0(x_0, y_0)|\, \mathrm{d}x_0\, \mathrm{d}y_0. \tag{2.15}$$

Obviously, (2.15) provides the better estimation of the upper bound of $|\overline{M}|$ than equation (2.12). Physically (2.15) means that for a given sign-defined initial PV distribution the modulus of the total mass $|\overline{M}|$ is maximal if the disturbance is

elongated parallel to the boundary at the level $y = \bar{y}_e$, i.e. if all fluid particles are at the equal distance $\bar{y}_e$ from the wall.

Restriction on $|\overline{M}|$ from below follows from the energy conservation:

$$\int_{y>0} \Psi Q \, \mathrm{d}x \, \mathrm{d}y = -2E = \text{const.} \tag{2.16}$$

One can readily obtain from (2.16) that

$$\int_{y>0} |\Psi| \, \mathrm{d}x \, \mathrm{d}y \geqslant \frac{2E}{|Q_0|_{\max}}. \tag{2.17}$$

If Q_0 is of one sign then the streamfunction Ψ is also of one sign (opposite to the sign of Q_0) by virtue of the equation $Q = \nabla^2\Psi - \Psi$ and PV conservation. Therefore, for this case we have

$$|\overline{M}| = \int_{y>0} |\Psi| \, \mathrm{d}x \, \mathrm{d}y \geqslant \frac{2E}{|Q_0|_{\max}}. \tag{2.18}$$

Thus, the total geostrophic mass $\overline{M}$ is bounded in absolute value by the parameter $|\overline{M}_a|_{\max}$ (see (2.15)) from above and by the value $2E/|Q_0|_{\max}$ from below. Both bounds do not depend on time and are determined in terms of the initial conditions.

Restrictions (2.15), (2.18) provide a rough estimate of the variability of the total geostrophic mass given a sign-defined initial PV. Of course, these estimates do not take into account details of dynamics described by (1.4*d*); therefore, maximum (2.15) and minimum (2.18) are hardly achieved in the general case. However, maximum (2.15) can be achieved in the simplest case of two point vortices (see § 3). Also, (2.15) turns out to be useful for interpreting the numerical experiments in § 4.

3. System of two point vortices

It was shown in § 2.1 that the total mass of localized QG perturbation changes in time if (i) the perturbation is not steadily translated along the wall, and (ii) the fluid particles with non-zero PV are displaced perpendicular to the boundary $y = 0$. Obviously, the simplest system possessing these properties consists of two point vortices interacting with each other and with the wall; the dynamics of this system are analysed below. General equations governing the system of N point vortices interacting with the wall are represented in Appendix C; for $N = 2$ the system of equations (C 4) for the vortex trajectories takes the form

$$\dot{x}_1 = \frac{A_1}{2\pi} K_1(2y_1) + \frac{A_2}{2\pi}\left[\frac{\bar{y}_{12}K_1(\bar{r}_{12})}{\bar{r}_{12}} - \frac{y_{12}K_1(r_{12})}{r_{12}}\right], \tag{3.1a}$$

$$\dot{y}_1 = \frac{A_2}{2\pi} x_{12}\left[\frac{K_1(r_{12})}{r_{12}} - \frac{K_1(\bar{r}_{12})}{\bar{r}_{12}}\right], \tag{3.1b}$$

$$\dot{x}_2 = \frac{A_2}{2\pi} K_1(2y_2) + \frac{A_1}{2\pi}\left[\frac{\bar{y}_{12}K_1(\bar{r}_{12})}{\bar{r}_{12}} + \frac{y_{12}K_1(r_{12})}{r_{12}}\right], \tag{3.1c}$$

$$\dot{y}_2 = \frac{A_1}{2\pi} x_{12}\left[\frac{K_1(\bar{r}_{12})}{\bar{r}_{12}} - \frac{K_1(r_{12})}{r_{12}}\right]. \tag{3.1d}$$

Here $x_i = x_i(t)$, $y_i = y_i(t)$, $i = 1, 2$, are the vortex coordinates, subscript i denotes the vortex number, $x_{12} = x_1 - x_2$, $y_{12} = y_1 - y_2$, $\bar{y}_{12} = y_1 + y_2$, and

$$r_{12} = \sqrt{x_{12}^2 + y_{12}^2}, \; \bar{r}_{12} = \sqrt{x_{12}^2 + (y_1 + y_2)^2}. \tag{3.2a, b}$$

Relationship (C 5) can be written as follows

$$A_1 y_1 + A_2 y_2 = (A_1 + A_2) y_c, \tag{3.3}$$

where y_c is a constant distance from the vortex pair centroid to the wall. Mass $\overline{M}_2$ and its time derivative $\dot{\overline{M}}_2$ are expressed by

$$\overline{M}_2 = -A_1(1 - \mathrm{e}^{-y_1}) - A_2(1 - \mathrm{e}^{-y_2}), \tag{3.4a}$$

$$\dot{\overline{M}}_2 = \frac{A_1 A_2}{4\pi} x_{12} \left[\frac{K_1(r_{12})}{r_{12}} - \frac{K_1(\bar{r}_{12})}{\bar{r}_{12}} \right] (\mathrm{e}^{-y_1} - \mathrm{e}^{-y_2}). \tag{3.4b}$$

The set of equation (3.1) is readily reduced to two equations for the distances between the vortices x_{12}, y_{12}:

$$\dot{x}_{12} = \overline{A}_1 K_1(2y_1) - \overline{A}_2 K_1(2y_2) - (\overline{A}_1 + \overline{A}_2) \frac{y_{12} K_1(r_{12})}{r_{12}} + (\overline{A}_2 - \overline{A}_1) \frac{\bar{y}_{12} K_1(\bar{r}_{12})}{\bar{r}_{12}}, \tag{3.5a}$$

$$\dot{y}_{12} = (\overline{A}_1 + \overline{A}_2) x_{12} \left[\frac{K_1(r_{12})}{r_{12}} - \frac{K_1(\bar{r}_{12})}{\bar{r}_{12}} \right] \tag{3.5b}$$

where $\overline{A}_k = A_k/2\pi$, $k = 1, 2$. The coordinates y_1, y_2 in (3.5) are expressed in terms of the constant y_c and variable y_{12} using equation (3.3):

$$y_1 = y_c + \frac{\overline{A}_2}{\overline{A}_1 + \overline{A}_2} y_{12}, \quad y_2 = y_c - \frac{\overline{A}_1}{\overline{A}_1 + \overline{A}_2} y_{12}. \tag{3.6a, b}$$

Equations (3.5), (3.6) allow calculation of the variables x_{12}, y_{12}, y_1, y_2 depending on the time t and, therefore, the mass $\overline{M}_2$. To obtain the phase portraits (the relation between x_{12} and y_{12}) of system (3.5), (3.6) we use the energy conservation integral, which is written as follows:

$$2A_1 A_2 [K_0(r_{12}) - K_0(\bar{r}_{12})] - A_1^2 K_0(2y_1) - A_2^2 K_0(2y_2) = \text{const}. \tag{3.7}$$

Typical behaviour of the vortex pair near the rectilinear wall is presented in figures 1–3. The phase portraits (part (a)) indicate that if the initial distance between the vortices is sufficiently small, then the vortices move periodically, rotating around some moving centre.

Correspondingly, the total mass $\overline{M}_2$ and its time derivative $\dot{\overline{M}}_2$ are periodical functions of time (part (b)). In the case when the amplitudes A_1, A_2 are of the same sign (figures 1 and 2), the minimal values of $\overline{M}_2$ (see part (b)) are equal to $-|\overline{M}_2^{(a)}|$. To determine the maximum values of $\overline{M}_2$ we use the fact that in accordance with (3.4b) (see also part (c)) the time derivative $\dot{\overline{M}}_2$ vanishes at two points: at the point $y_1 = y_2$ which corresponds to the minima of mass, and at the point $x_1 = x_2$ corresponding to the maxima of mass $\overline{M}_2$. Thus, we come to the simple rule: the absolute value of the mass of the two-point vortex system is maximal when the system is elongated along the wall and minimal for the system elongated perpendicular to the wall. An analogous effect occurs for the distributed perturbations (see the next Section).

If the initial distance is sufficiently large, then the motion of the pair is non-periodic, with the distance between the vortices increasing monotonically from some time on. Correspondingly, the interaction between the vortices weakens and as time passes, the vortices move practically rectilinearly and uniformly along the boundary. The total mass $\overline{M}_2$ and derivative $\dot{\overline{M}}_2$ tend to some constant value and to zero, respectively, with increasing time.

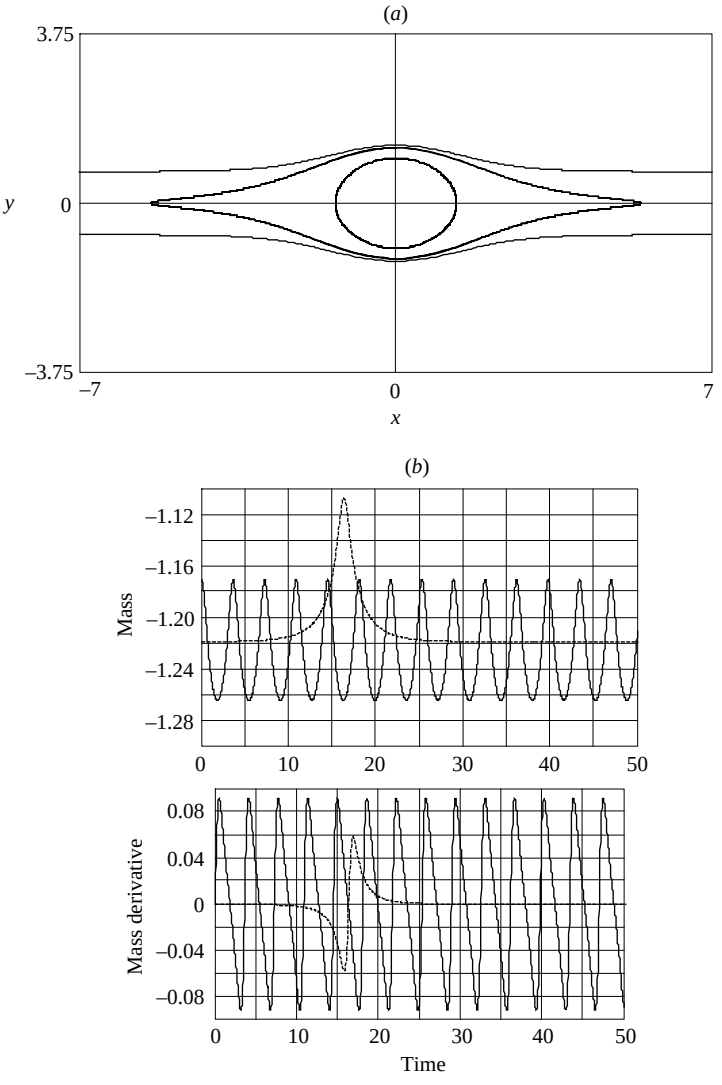

FIGURE 1. Behaviour of a pair of point vortices of the same magnitude and sign interacting with *a* wall. (*a*) The phase plot of the system, for $\overline{A}_1 = 1$, $\overline{A}_2 = 1$, $y_0 = 1$. (*b*) Time evolution of the total mass of the pair. The oscillating curves correspond to small distances between the vortices or closed phase trajectories. The other curve corresponds to open phase trajectories.

The shapes of the phase trajectories depend substantially on the vortex signs. If the vortices are of the same sign, then the periodic trajectories are lens-like, with the longitudinal size of the lens (along the x-axis) increasing and tending to infinity as its transversal size (along the y-axis) tends to some limiting value Δ. For example if $\overline{A}_1 = \overline{A}_2 = 1$, the parameter $\Delta = 2.4516$. The 'limit' of an infinitely long lens is a separatrix between periodic and non-periodic regimes.

In the case of the vortices having opposite signs, the shape of the phase trajectories is more 'usual' and the separatrix is a loop with two infinite 'tendrils' (see figure 3). We note that this phase portrait is valid only if the vortex amplitudes are different, i.e. $|\overline{A}_1| \neq |\overline{A}_2|$. If $\overline{A}_1 = -\overline{A}_2$, then the periodic regimes are impossible.

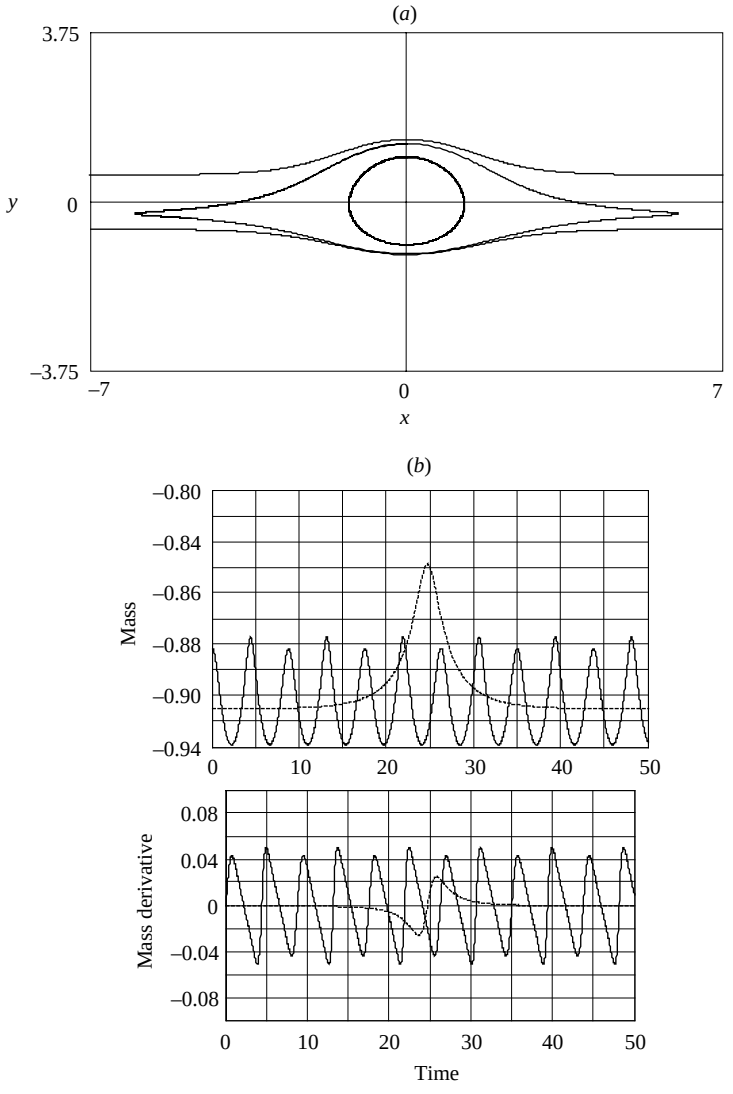

FIGURE 2. The same as in figure 1 except that the vortices are of different amplitude: $\overline{A}_1 = 0.5$, $\overline{A}_2 = 1$.

Thus, the total mass of two point vortices interacting near a wall either oscillates periodically in time in the vicinity of some mean value (small distance between the vortices) or tends to some constant (large distance between the vortices). In the case of three point vortices (not shown) the total mass behaves analogously, but the oscillating regime, generally, is not periodic.

What is the evolution of mass of a system of distributed vortices? Let the vortices be monopoles and the distance between them greatly exceed their typical sizes. One can assume that in this case the system behaviour would be qualitatively the same as the behaviour of the system of point vortices. But if the vortex size is comparable to the distance between them, then changes in the vortex structure can affect the total mass of the system. To study this effect we consider numerical experiments with various localized initial states.

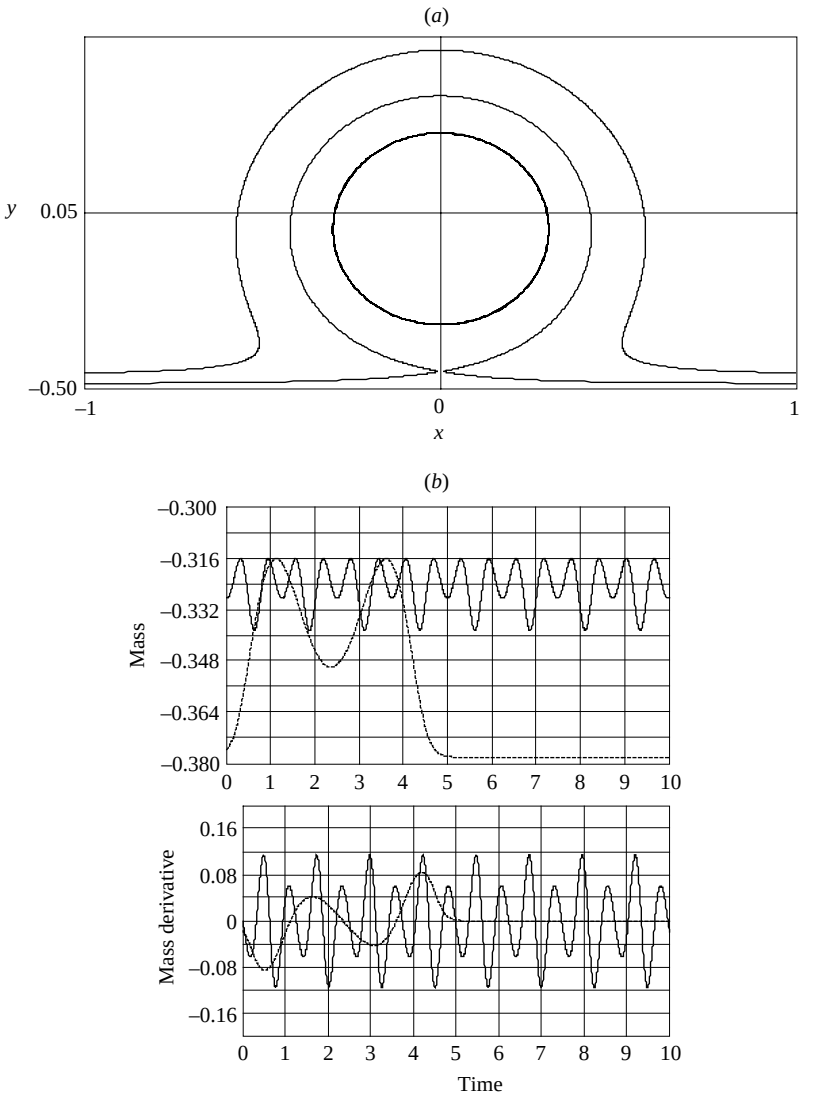

FIGURE 3. The same as in figure 1 except that the point vortices are of different sign: $\overline{A}_1 = -0.5$, $\overline{A}_2 = 1$.

4. Numerical experiments with distributed vortices

In the numerical model for equation (1.4*d*), the Arakawa scheme was used to represent the Jacobian; the time derivative was approximated either by central differences or by the Adams–Bashforth formula. Biharmonic viscosity provided a sink for the small-scale vorticity. The calculations were made for a channel bounded by two solid walls at $y = 0, L$, the motion along the channel (x-axis) being assumed to be periodic. The no-flux condition $\Psi = 0$ at $y = 0, L$ and the no-slip condition $Q = 0$ at $y = 0, L$ were used at the channel boundaries. The initial perturbation was located near the south boundary $y = 0$; the channel width L and period along the x-axis were sufficiently large to neglect the interaction of the perturbation with the north wall $y = L$ and adjacent boxes. Numerical experiments with various initial

perturbations showed that the total mass is rather robust, depending weakly on space–time resolution and the domain size.

The initial streamfunction Ψ_0 in the experiments was calculated given initial potential vorticity Q_0 by solving the equation

$$\nabla^2\Psi_0 - \Psi_0 = Q_0, \tag{4.1}$$

where Q_0 is conveniently determined by the finite-area function

$$F(z) = \begin{cases} \dfrac{A}{z}\left(\dfrac{J_1(kz)}{J_1(ka)} - \dfrac{z}{a}\right), & z < a \\ 0, & z \geqslant a. \end{cases} \tag{4.2}$$

Here A, k, and a are constants; $J_1(z)$ denotes the first-order Bessel function, and the variable z is defined by

$$z = \sqrt{\frac{x^2}{s^2} + (y-d)^2}, \tag{4.3}$$

where s determines the perturbation size along the x-axis and d is the distance of the centre of the perturbation from the boundary $y = 0$. For $s < 1$ the perturbation is elongated along the y-axis; for $s > 1$ it is elongated along the x-axis. In numerical experiments represented in figures 4–7 the following parameter values were adopted: $A = 2$, $k = 5.136$, $a = 1$, $d = 1$.

For a vortex dipole the initial PV was prescribed in the form

$$Q_0 = \frac{y-d}{z}F(z), \quad s = 1. \tag{4.4}$$

The dipole evolution is qualitatively similar to the evolution of pair of point vortices of opposite sign (figure 4). Interaction with the boundary results in the destruction of the dipole, the vortices gradually move apart, and the pair eventually splits into two monopoles moving in opposite directions along the boundary. Correspondingly, the total mass increases and tends to a new constant value with increasing time. The change in the total mass exceeds 50% of its initial value in this case, i.e. it is quite significant.

The evolution of the pair of vortices of the same sign was examined for the initial state

$$Q_0 = \frac{|y-d|}{z}F(z), \ \ s = 1. \tag{4.5}$$

The vortices rotate around some common centre, elongate and deform as is seen from the evolution of PV field (figure 5). The total mass variability in this case is substantially less than for the dipole. The main change of the mass takes place during the initial adaptation period, then the pair transforms into an approximately axisymmetric vortex and the mass oscillates with small amplitude near its mean value. The mass is maximal at $T = 1$ (minimal at $T = 0$) when the perturbation is elongated along (perpendicular to) the wall, as was found for the point vortex pair in the previous Section.

Thus, in both these cases the vortex system evolution results in one or two monopole vortices interacting with the boundary. We carried out special numerical experiments to study the dynamics of the monopoles near the wall. The calculations were made for an initially circular vortex with $Q_0 = F(z)$, $s = 1$ (figure 6) and for a vortex initially elongated along the y-axis with $Q_0 = F(z)$, $s = 0.5$ (figure 7). In both these cases the vortex mass oscillates in time similarly to the total mass of two same-sign point

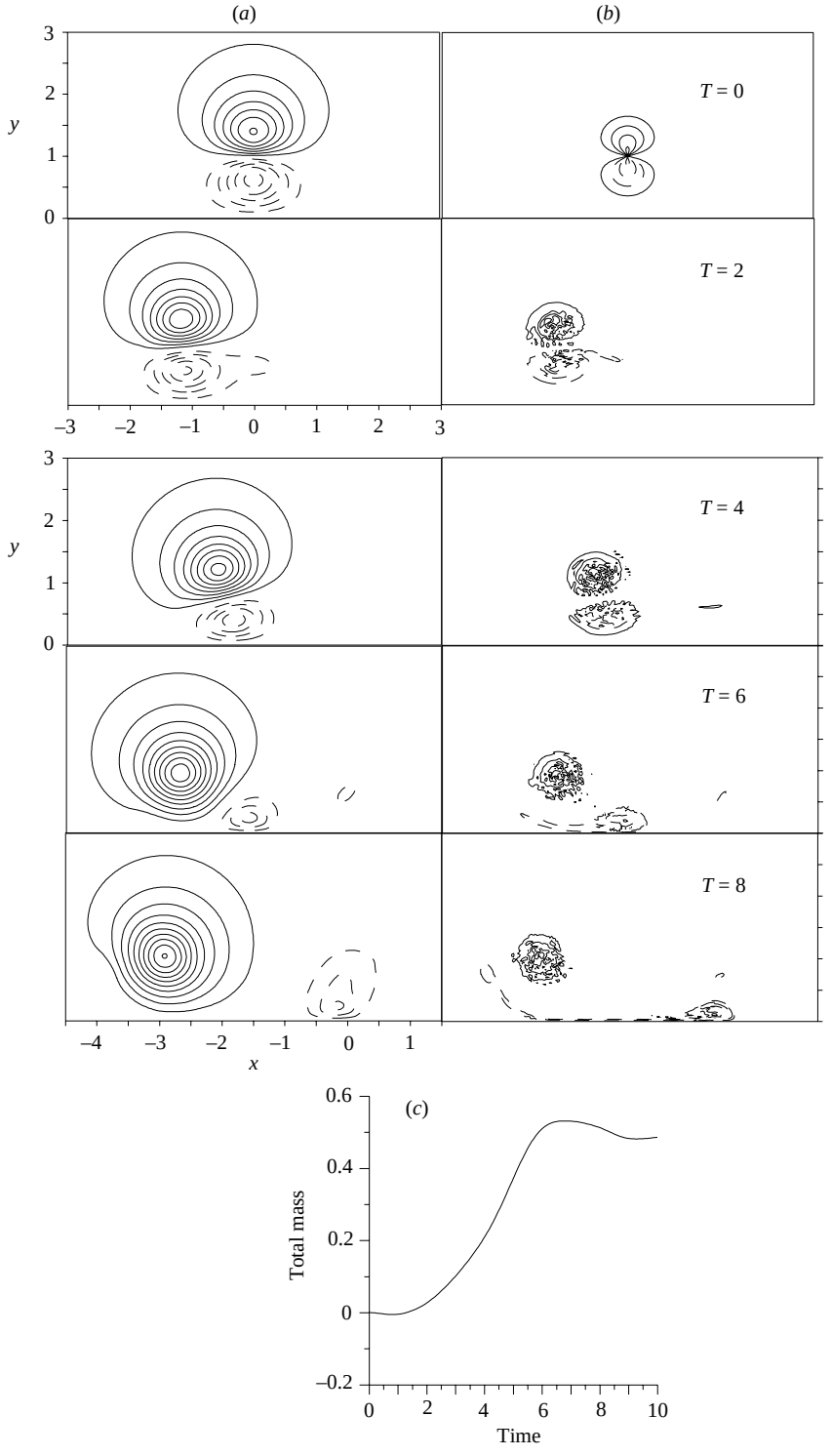

FIGURE 4. Evolution of the distributed dipole (4.4). (*a*) The stream function and (*b*) the potential vorticity contours for different time T. The normalized deviation of mass $(M - M_1)/M_1$ from its initial value M_1 is shown in (*c*).

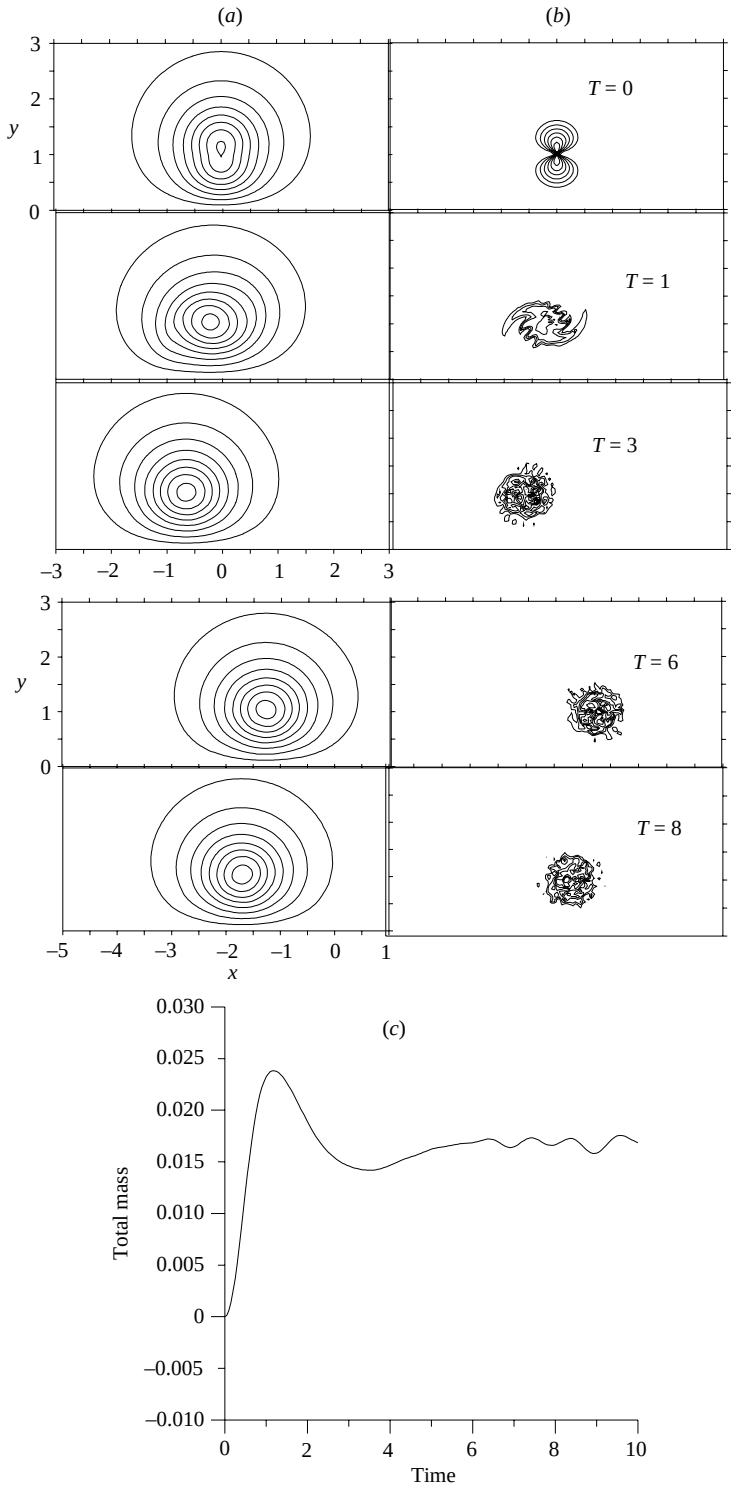

FIGURE 5. The same as in figure 4 except that it is for the distributed vortex pair (4.5).

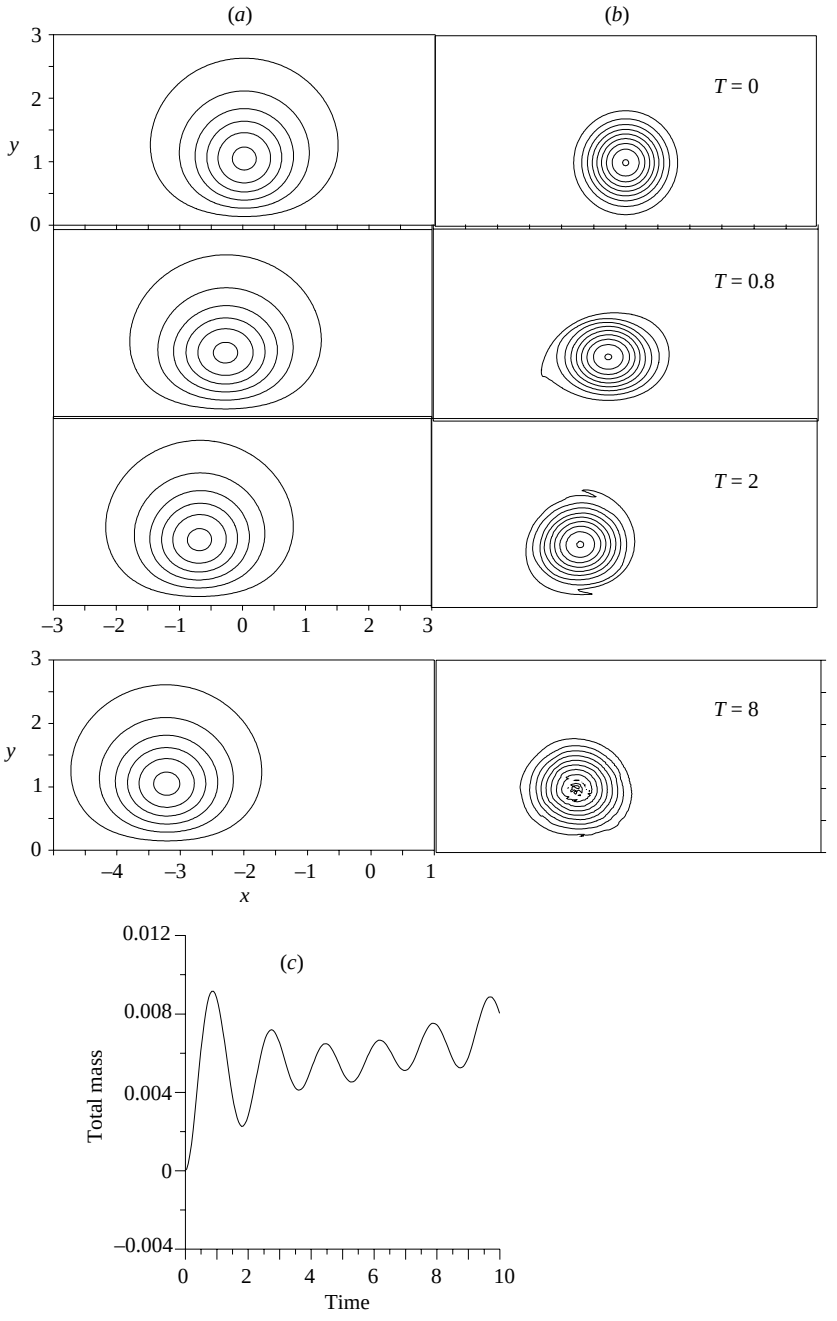

FIGURE 6. The same as in figure 4 except that it is for the initially circular vortex; $Q_0 = F(z)$, $s = 1$.

vortices separated by a small distance. The variability of mass of the elongated vortex is somewhat larger than of the circular one, which is obviously related to larger displacements of fluid particles along the y-axis when the elongated vortex is rotating around its centre. Again, the total mass is minimal (maximal) when the perturbation is elongated perpendicular to (along) the wall.

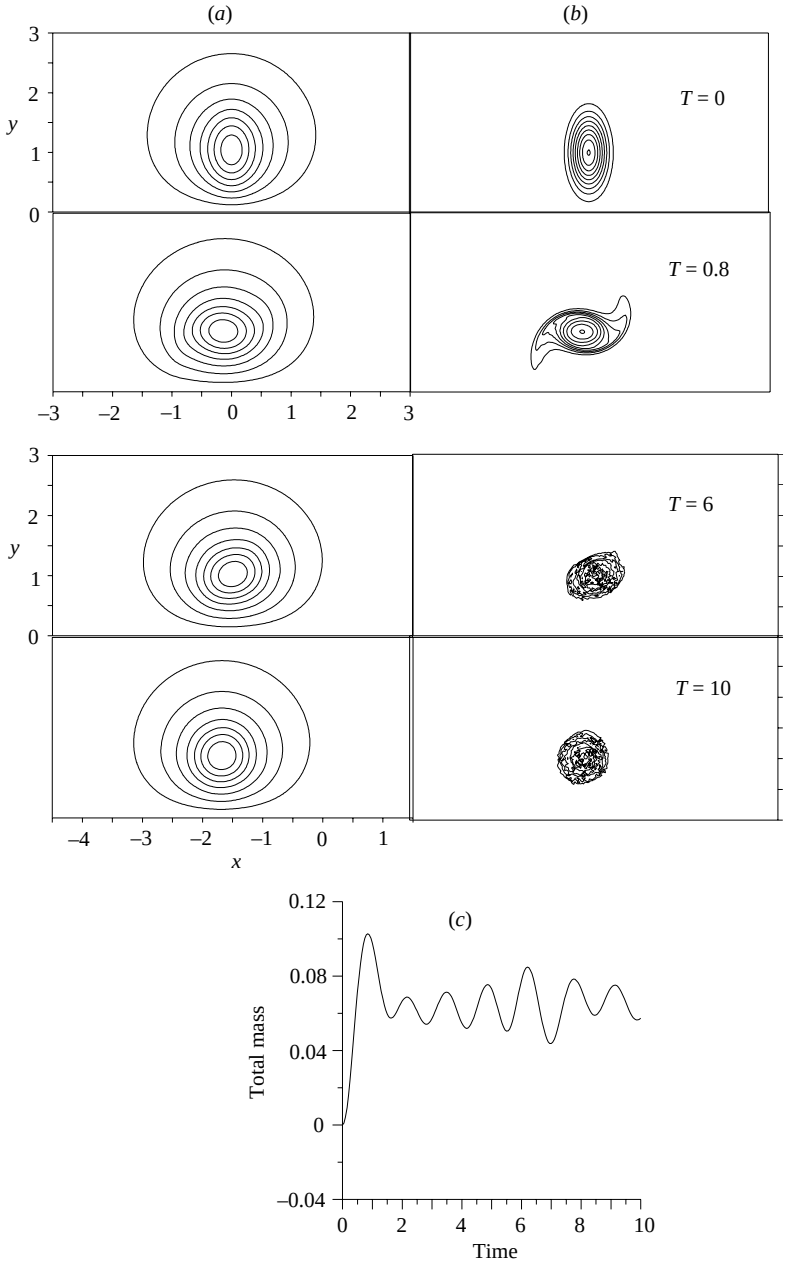

FIGURE 7. The same as in figure 4 except that it is for the vortex elongated along the y-axis; $Q_0 = F(z)$, $s = 0.5$.

It should be noted that the amplitude of mass oscillations for the monopoles, being rather small, remains nearly the same after the initial adaptation and this is almost independent of the time and spatial resolution of our numerical scheme with small viscosity. By virtue of the symmetry of the problem (1.4*d*), (1.5), (1.9) the monopole evolution is equivalent to the evolution of the dipole composed of the vortex and its 'image' on the unbounded plane. The above-described non-decaying oscillations

of the vortices in the dipole indicate that their inviscid evolution may not tend to a stationary limit.

5. First-order correction

Analytical calculations and numerical simulations in the preceding Sections show that the mass of localized QG disturbance varies in time. At the same time, the total (geostrophic + ageostrophic) mass in the full RSW model (which the QG equations follow for small Rossby numbers) should be conserved. To provide the mass conservation we have to take into account the fast ageostrophic waves, i.e. to relax the assumption that the motion is slow. The non-dimensional equations of the RSW model take the following form (cf. (1.1)):

$$\frac{\partial U}{\partial t}+\varepsilon\left(U\frac{\partial U}{\partial x}+V\frac{\partial U}{\partial y}\right)-V=-\frac{\partial P}{\partial x}, \tag{5.1a}$$

$$\frac{\partial V}{\partial t}+\varepsilon\left(U\frac{\partial V}{\partial x}+V\frac{\partial V}{\partial y}\right)+U=-\frac{\partial P}{\partial y}, \tag{5.1b}$$

$$\frac{\partial \Pi}{\partial t}+\varepsilon\left\{\frac{\partial(U\Pi)}{\partial x}+\frac{\partial(V\Pi)}{\partial y}\right\}=0. \tag{5.1c}$$

The solution obeys the no-flux condition (1.2).

Here we consider localized and geostrophically balanced initial fields, i.e.

$$P=\Psi_I(x,y), U=U_I(x,y)=-\frac{\partial \Psi_I}{\partial y}, V=V_I(x,y)=\frac{\partial \Psi_I}{\partial x} \text{ at } t=0. \tag{5.2}$$

Following RG we represent the solution in the form of the asymptotic expansions:

$$U=U_0(x,y,t,T,T_2\ldots)+\varepsilon u(x,y,t,T,T_2\ldots)+\cdots, \tag{5.3a}$$

$$V=V_0(x,y,t,T,T_2\ldots)+\varepsilon v(x,y,t,T,T_2\ldots)+\cdots, \tag{5.3b}$$

$$P=\Psi(x,y,t,T,T_2\ldots)+\varepsilon h(x,y,t,T,T_2\ldots)+\cdots. \tag{5.3c}$$

Here $T=\varepsilon t$, $T_n=\varepsilon^n t$, $n=2,3\ldots$, are the slow times introduced to prevent the solution from a secular growth in time.

Due to geostrophically balanced initial conditions (5.2), at the lowest order the solution does not depend on the fast time t and obeys the geostrophic relationships

$$U_0=-\frac{\partial \Psi}{\partial y}, \quad V_0=\frac{\partial \Psi}{\partial x}; \quad \Psi=\Psi(x,y,T,\ldots). \tag{5.4}$$

To describe the first-order solution, we obtain from (5.1)–(5.3) the equations

$$\frac{\partial u}{\partial t}-v+\frac{\partial h}{\partial x}=R_u, \frac{\partial v}{\partial t}+u+\frac{\partial h}{\partial y}=R_v, \frac{\partial(\varsigma-h)}{\partial t}=R_\varsigma, \tag{5.5a–c}$$

$$v|_{y=0}=0, (u,v,h)_{t=0}=0, \tag{5.5d, e}$$

$$R_u=\left(\frac{\partial}{\partial T}-\frac{\partial \Psi}{\partial y}\frac{\partial}{\partial x}+\frac{\partial \Psi}{\partial x}\frac{\partial}{\partial y}\right)\frac{\partial \Psi}{\partial y}, R_v=-\left(\frac{\partial}{\partial T}-\frac{\partial \Psi}{\partial y}\frac{\partial}{\partial x}+\frac{\partial \Psi}{\partial x}\frac{\partial}{\partial y}\right)\frac{\partial \Psi}{\partial x}, \tag{5.6a, b}$$

$$R_\varsigma=-\frac{\partial(\nabla^2\Psi-\Psi)}{\partial T}-J(\Psi,\nabla^2\Psi). \tag{5.6c}$$

Here $\varsigma-h=\partial_x v-\partial_y u-h$ is the first-order potential vorticity.

The streamfunction Ψ does not depend on the fast time t, and therefore, by virtue of (5.5c) for $\varsigma - h$ to be bounded as $t \to \infty$, the function R_ς must be identically zero,

$$R_\varsigma = 0, \tag{5.7}$$

whence we obtain that Ψ satisfies equation (1.4d).

Taking into account (5.7), we obtain the first-order mass conservation equation from (5.5a–c) in the form

$$\frac{\partial h}{\partial t} + \frac{\partial u}{\partial x} + \frac{\partial v}{\partial y} = \frac{\partial R_v}{\partial x} - \frac{\partial R_u}{\partial y}, \tag{5.8}$$

which shows that changes of the first-order total mass $M_1 = \int_{y>0} h \, \mathrm{d}x \, \mathrm{d}y$ in the localized case are expressed as

$$\frac{\partial M_1}{\partial t} = \int_{-\infty}^{\infty} R_u(x, 0, t) \, \mathrm{d}x = \int_{-\infty}^{\infty} \left. \frac{\partial^2 \Psi}{\partial y \partial T} \right|_{y=0} \mathrm{d}x. \tag{5.9}$$

We see that these changes compensate exactly the changes of the lowest-order geostrophic mass given by (2.2). Therefore, instead of splitting the solution to (5.5), (5.6) into the fast and slow components used in RG, here we represent it as a sum

$$(u, v, h) = (u_c, v_c, h_c) + (u_j, v_j, h_j), \tag{5.10}$$

where the components conserving the corresponding total mass fields u_c, v_c, h_c obey the equations

$$\frac{\partial u_c}{\partial t} - v_c + \frac{\partial h_c}{\partial x} = R_u' = R_u - e^{-y} \left. \frac{\partial^2 \Psi}{\partial y \partial T} \right|_{y=0}, \frac{\partial v_c}{\partial t} + u_c + \frac{\partial h_c}{\partial y} = R_v, \frac{\partial (\varsigma_c - h_c)}{\partial t} = 0, \tag{5.11a–c}$$

$$v_c|_{y=0} = 0, \quad (u_c, v_c, h_c)_{t=0} = 0, \tag{5.11d, e}$$

while the residual fields u_j, v_j, h_j responsible for the mass changes (5.9) satisfy the system

$$\frac{\partial u_j}{\partial t} - v_j + \frac{\partial h_j}{\partial x} = e^{-y} \left. \frac{\partial^2 \Psi}{\partial y \partial T} \right|_{y=0}, \frac{\partial v_j}{\partial t} + u_j + \frac{\partial h_j}{\partial y} = 0, \frac{\partial (\varsigma_j - h_j)}{\partial t} = 0, \tag{5.12a–c}$$

$$v_j|_{y=0} = 0, (u_j, v_j, h_j)_{t=0} = 0. \tag{5.12d, e}$$

Analysis of system (5.11) is performed exactly in the same way as in § 5 of RG and reveals that the fields u_c, v_c, h_c are localized; therefore, they are unimportant if we are interested in the leading-order solution.

The solution to system (5.12) is sought in the form

$$(u_j, v_j, h_j) = (\phi_j, 0, \phi_j) \, \mathrm{e}^{-y}, \tag{5.13}$$

which satisfies no-flux boundary condition (5.12d). The evolution of ϕ_j is described by the equation

$$\frac{\partial \phi_j}{\partial t} + \frac{\partial \phi_j}{\partial x} = \left. \frac{\partial^2 \Psi}{\partial y \partial T} \right|_{y=0}. \tag{5.14}$$

The solution for ϕ_j satisfying zero initial condition is written as

$$\phi_j(x, t, T) = \int_{x-t}^{x} \left. \frac{\partial^2 \Psi}{\partial y \partial T} \right|_{y=0} \mathrm{d}x'. \tag{5.15}$$

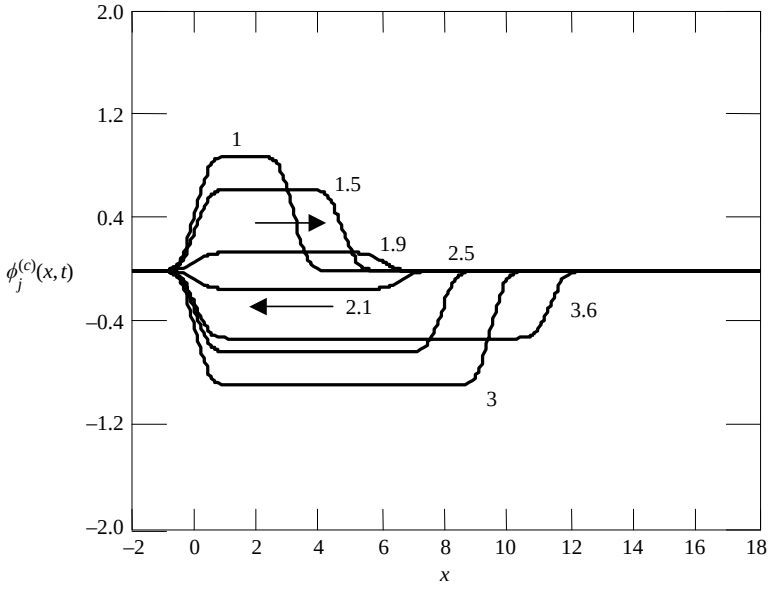

FIGURE 8. Schematic representation of the time evolution of the compensating jet in the oscillating regime. Plots of the amplitude $\phi_j^{(c)}$ in (5.21) are shown for different times for the model case

$$\int_{-\infty}^{\infty} \partial^2\Psi/\partial y\partial T|_{y=0}\,\mathrm{d}x = (\sqrt{\pi}/2)\sin(0.5t)$$

with function $\varphi(x) = (2/\sqrt{\pi})\exp(-4x^2)$. Numbers near the curves denote the scaled time t/π. It is seen that the jet length increases monotonically with time and its intensity oscillates, changing its sign. Arrows show the direction of the jet velocity.

It follows from (5.14) that the solution (5.13), (5.15) can be interpreted as a forced Kelvin wave generated by the along-wall slow velocity varying in time. This wave looks like an injected jet propagating along the wall to the right of the localized lowest-order disturbance as shown in figures 8 and 9. The time derivative of the total mass of the jet is equal to

$$\frac{\partial}{\partial t}\int_{y>0} \mathrm{e}^{-y}\phi_j\,\mathrm{d}x\,\mathrm{d}y = \int_{-\infty}^{\infty} \frac{\partial^2\Psi}{\partial y\partial T}\bigg|_{y=0}\mathrm{d}x = -\frac{\partial\overline{M}}{\partial T}. \tag{5.16}$$

Comparing (2.2) to (5.16) we conclude that this compensating jet takes away the surplus or shortage (depending on the sign of $\partial\overline{M}/\partial T$) of the mass from the localized lowest-order disturbance; if the geostrophic mass $\overline{M}$ decreases (increases), then the jet velocity u_j is positive (negative) for sufficiently large x and $t \gg x$.

We now consider the dynamics of compensating jet (5.13) in detail, representing the amplitude ϕ_j in the form

$$\phi_j = \int_{x-t}^{x} a(x,T)\,\mathrm{d}x + \left[\int_{-\infty}^{\infty} \frac{\partial^2\Psi}{\partial y\partial T}\right]_{y=0}\int_{x-t}^{x}\varphi(x)\,\mathrm{d}x, \tag{5.17}$$

where

$$a(x,T) = \left[\frac{\partial^2\Psi}{\partial y\partial T} - \varphi(x)\int_{-\infty}^{\infty}\frac{\partial^2\Psi}{\partial y\partial T}\right]_{y=0}, \tag{5.18}$$

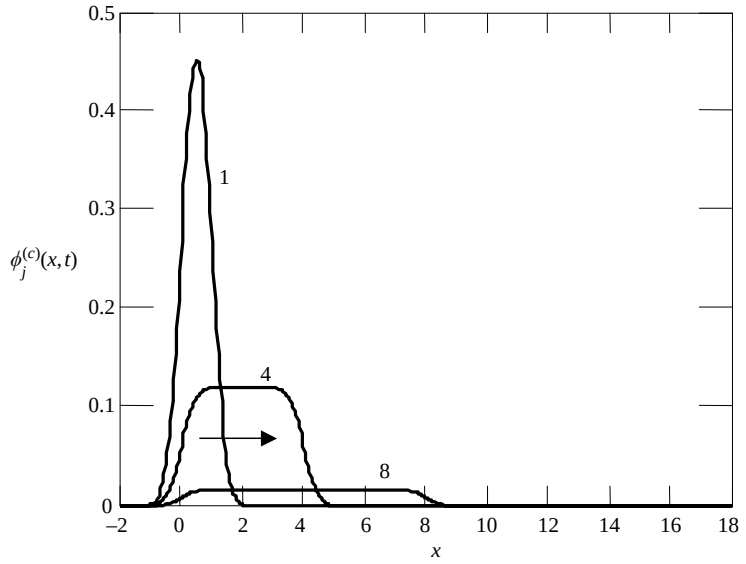

FIGURE 9. The same as in figure 8 except that it is for the 'limiting' regime. It is seen that the jet length also increases monotonically with time while its intensity gradually tends to zero.

and $\varphi(x)$ is an arbitrary localized function satisfying the condition

$$\int_{-\infty}^{\infty} \varphi(x)\,\mathrm{d}x = 1. \tag{5.19}$$

The function $a(x, T)$ is also localized in x and

$$\int_{-\infty}^{\infty} a(x, T)\,\mathrm{d}x = 0 \tag{5.20}$$

by virtue of (5.19). One can readily show that the first term on the right-hand side of (5.17) does not make any contribution to the integral on the left-hand side of (5.16) and the mass conservation is provided by the second term on the right-hand side of (5.17),

$$\phi_j^{(c)} = \left[\int_{-\infty}^{\infty} \frac{\partial^2 \Psi}{\partial y \partial T}\right]_{y=0} \int_{x-t}^{x} \varphi(x)\,\mathrm{d}x = -\frac{\partial \overline{M}}{\partial T} \int_{x-t}^{x} \varphi(x)\,\mathrm{d}x. \tag{5.21}$$

For example, we can choose the function $\varphi(x)$ as

$$\varphi(x) = \frac{c}{\sqrt{\pi}} \mathrm{e}^{-c^2 x^2}, \tag{5.22}$$

where c is a constant. Note that the arbitrariness of $\varphi(x)$ is related to the fact that representation of a function as a sum of localized and non-localized parts is not uniquely defined.

Integral $\int_{x-t}^{x} \varphi(x)\,\mathrm{d}x$ represents the along-wall jet expanding with the constant speed of a Kelvin wave to the right of the initial perturbation. The slow time-dependent amplitude $-\partial \overline{M}/\partial T$ (time rate of the total mass with a minus) determines the jet sign and intensity at each moment. In the oscillating regime the jet sign and intensity also slowly (in comparison with the jet propagation) oscillate as shown in figure 8. The limiting regime is represented in figure 9. In this case the jet sign does not change and the jet amplitude slowly tends to zero.

6. Comparison of localized and periodically localized solutions

We have considered the situation when a localized disturbance interacts with an infinitely long boundary and shown that the QG component of the motion obeys the zero boundary condition for the QG streamfunction. In the case of periodic motion or motion in a finite domain the boundary conditions for the QG component are more complicated: the boundary streamfunction is an unknown function of the slow time T and is determined using the condition of conservation of circulation of the along-wall QG velocity (see e.g. Phillips 1954, McWilliams 1977 and below). It is possible, however, that for some conditions the zero boundary conditions for the QG streamfunction can be used approximately, if the motion is sufficiently localized and the domain is sufficiently large. The using of zero boundary conditions for the QG component instead of more complicated ones will be referred to as the approximation of an infinite domain. An important question is: what are the conditions for the approximation of infinite domain to be applied? To answer this question we need to investigate the evolution of a localized perturbation in a bounded domain having a size greatly exceeding the typical size of the perturbation. However, the problem of geostrophic adjustment in a closed basin is not yet solved even for the linear case. Instead, we consider problem (5.1) with periodic initial conditions of the form

$$\Psi_I^{(P)} = \sum_{n=-\infty}^{\infty} \Psi_I^{(L)}(x + nL_x, y), \tag{6.1}$$

where $\Psi_I^{(L)}(x, y)$ is a localized function sufficiently rapidly decaying at $x \to \pm\infty$, $y \to \infty$; L_x is the period. Superscripts (P), (L) here and below denote the periodic and localized solutions, respectively. For convenience initial condition (6.1) and the corresponding solution $\Psi^{(P)}(x, y, t)$ will be referred to as periodically localized.

The primary aim here is to compare the solutions of the localized problem for initial streamfunction $\Psi_I^{(L)}(x, y)$ with the periodically localized problem for initial streamfunction (6.1). Such a comparison, being interesting per se, allows us to better understand the evolution of localized disturbances in closed domains.

The solution to the RSW system (5.1) for periodic initial conditions is represented in the same way as in the preceding Section; equations (5.1) to (5.15) (excluding (5.9)) remain valid in the periodic case. The main difference is in boundary conditions for the QG equation (1.4*d*). For periodic QG motion condition (1.9) should be replaced by the more 'general' condition:

$$\Psi^{(P)} = \Psi^{(B)}(T) \text{ at } y = 0, \tag{6.2a}$$

where $\Psi^{(B)}(T)$ is an unknown function of the slow time. Because the amplitude (5.15) of the forced Kelvin wave as $t \to \infty$ must remain finite, another boundary condition is

$$\int_0^{L_x} \left. \frac{\partial^2 \Psi^{(P)}}{\partial y \partial T} \right|_{y=0} \mathrm{d}x = 0 \tag{6.2b}$$

(it is easy to check that if (6.2*b*) is not satisfied, then ϕ_j grows linearly in time). Note that traditionally, the condition (6.2*b*) is obtained from conservation of the QG velocity circulation or conservation of QG mass (e.g. Phillips 1954; McWilliams 1977; Kamenkovich & Reznik 1978). Simple analysis shows that the solution to system (5.11) is always periodic, bounded as $t \to \infty$, and does not impose additional restrictions on the lowest-order fields.

Thus, in the periodic case, the lowest-order QG component obeys equation (1.4*d*) and the usual boundary conditions (6.2*a*, *b*), but contrary to the localized case, the total QG mass in each periodic box is conserved.

Approximate localized and periodically localized solutions can be written in the same form; for example, for the geopotential we have

$$P^{(L)} \cong \Psi^{(L)} + \varepsilon \mathrm{e}^{-y} \int_{x-t}^{x} \left[\frac{\partial^2 \Psi^{(L)}}{\partial y \partial T} \right]_{y=0} \mathrm{d}x, \tag{6.3}$$

$$P^{(P)} \cong \Psi^{(P)} + \varepsilon \mathrm{e}^{-y} \int_{x-t}^{x} \left[\frac{\partial^2 \Psi^{(P)}}{\partial y \partial T} \right]_{y=0} \mathrm{d}x. \tag{6.4}$$

We neglect parts of the first-order solution which conserve mass and are insignificant physically when writing (6.3), (6.4).

We now represent the QG solution of periodic problem (1.4*d*), (6.2*a*, *b*) in the form

$$\Psi^{(P)} = \Psi_B(T)\mathrm{e}^{-y} + \tilde{\Psi}^{(P)}. \tag{6.5}$$

The function $\tilde{\Psi}^{(P)}$ obeys the equations

$$\frac{\partial\left(\nabla^2 \tilde{\Psi}^{(P)} - \tilde{\Psi}^{(P)}\right)}{\partial T} + J\left(\tilde{\Psi}^{(P)}, \nabla^2 \tilde{\Psi}^{(P)}\right) + \Psi_B \mathrm{e}^{-y} \frac{\partial\left(\nabla^2 \tilde{\Psi}^{(P)} - \tilde{\Psi}^{(P)}\right)}{\partial x} = 0, \tag{6.6a}$$

$$\tilde{\Psi}^{(P)}\big|_{y=0} = 0,\ \tilde{\Psi}^{(P)}\big|_{T=0} = \Psi_I^{(P)}. \tag{6.6b, c}$$

By virtue of (6.2*b*) the function Ψ_B is related to $\tilde{\Psi}^{(P)}$ in the following way:

$$\frac{\partial \Psi_B}{\partial T} = \frac{1}{L_x} \int_0^{L_x} \left. \frac{\partial^2 \tilde{\Psi}^{(P)}}{\partial y \partial T} \right|_{y=0} \mathrm{d}x. \tag{6.7}$$

We now construct an approximate solution to the problem (6.6), (6.7) for $L_x \gg 1$. At the initial moment $\Psi_B = 0$, $\partial \Psi_B / \partial T = O(1/L_x)$ (see Appendix B); therefore the solution is sought in the form of asymptotic expansions in the parameter $\delta = 1/L_x \ll 1$:

$$\tilde{\Psi}^{(P)} = \tilde{\Psi}_0^{(P)} + \delta \tilde{\Psi}_1^{(P)} + \cdots,\ \Psi_B = \delta \Psi_{B0} + \delta^2 \Psi_{B1} + \cdots. \tag{6.8a, b}$$

At the lowest order we have

$$\frac{\partial\left(\nabla^2 \tilde{\Psi}_0^{(P)} - \tilde{\Psi}_0^{(P)}\right)}{\partial T} + J\left(\tilde{\Psi}_0^{(P)}, \nabla^2 \tilde{\Psi}_0^{(P)}\right) = 0, \quad \tilde{\Psi}_0^{(P)}\big|_{y=0} = 0,\ \tilde{\Psi}_0^{(P)}\big|_{T=0} = \Psi_I^{(P)}, \tag{6.9a–c}$$

$$\frac{\partial \Psi_{B0}}{\partial T} = \int_0^{L_x} \left. \frac{\partial^2 \tilde{\Psi}_0^{(P)}}{\partial y \partial T} \right|_{y=0} \mathrm{d}x. \tag{6.9d}$$

If the initial function $\Psi_I^{(L)}$ is strongly localized, for example it behaves as $O(\mathrm{e}^{-r})$ for $r \to \infty$ then the localized solution $\Psi^{(L)}$ also behaves as $O(\mathrm{e}^{-r})$ for $r \to \infty$ (see Appendix B). Therefore, the approximate solution $\tilde{\Psi}_0^{(P)}$satisfying (6.9*a–c*) accurate within exponentially small terms $O(\mathrm{e}^{-1/\delta})$ can be written in the form

$$\tilde{\Psi}_0^{(P)} = \sum_{n=-\infty}^{\infty} \Psi^{(L)}(x + nL_x, y, T). \tag{6.10}$$

Substituting (6.10) into (6.9*d*) we obtain

$$\frac{\partial \Psi_{B0}}{\partial T} = \int_{-\infty}^{\infty} \left. \frac{\partial^2 \Psi^{(L)}}{\partial y \partial T} \right|_{y=0} \mathrm{d}x. \tag{6.11}$$

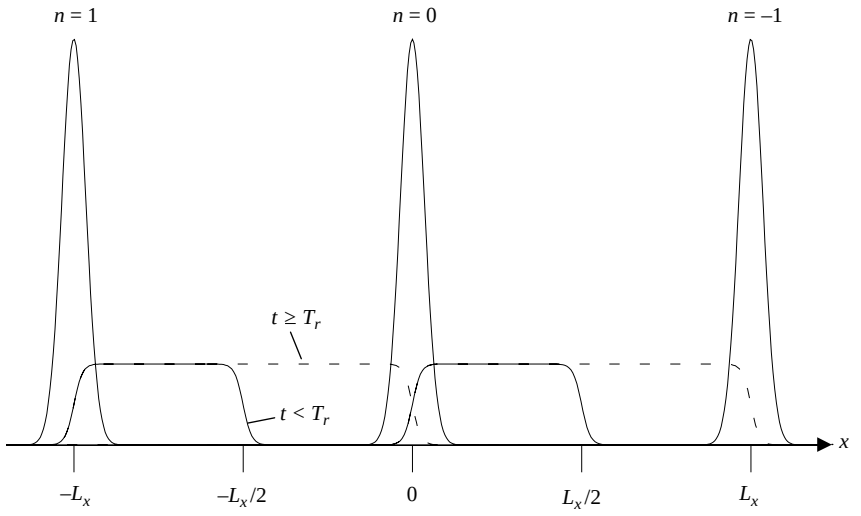

FIGURE 10. Schematic representation of the evolution of the periodically localized solution. Large peaks correspond to regions of localized motion, refers n to the box number. Propagation of the forced periodic Kelvin wave is shown at the time $t < T_r$ (solid line) when the approximation of an infinite domain can be still used, and at the time $t \geqslant T_r$ (dashed line) when condition (6.2) can be applied.

Using (6.8) the approximate solution (6.4) can be written as follows:

$$P^{(P)} \cong \tilde{\Psi}_0^{(P)} + \varepsilon \mathrm{e}^{-y} \int_{x-t}^{x} \left[\frac{\partial^2 \tilde{\Psi}_0^{(P)}}{\partial y \partial T} \right]_{y=0} \mathrm{d}x + \delta \mathrm{e}^{-y} \left[\Psi_{B0} - \varepsilon t \frac{\partial \Psi_{B0}}{\partial T} \right]. \tag{6.12}$$

We now consider the periodic solution (6.12) in the domain $|x| \leqslant L_x/2$, i.e. in the central box for $n = 0$ (see figure 10); because of periodicity, the analogous results will be valid for any box. Due to the rapid decay of $\Psi^{(L)}$ at infinity we have

$$\tilde{\Psi}_0^{(P)} = \Psi^{(L)} + O\left(\mathrm{e}^{-1/\delta}\right), |x| \leqslant L_x/2, \tag{6.13}$$

i.e. in this box the first term in (6.12) is close to the first term in localized solution (6.3).

Using (6.10), the integral in second term in (6.12) can be written as

$$J^{(P)} = \int_{x-t}^{x} \left[\frac{\partial^2 \tilde{\Psi}_0^{(P)}}{\partial y \partial T} \right]_{y=0} \mathrm{d}x = \sum_{-\infty}^{\infty} \int_{x-t+nL_x}^{x+nL_x} \left. \frac{\partial^2 \Psi^{(L)}}{\partial y \partial T} \right|_{y=0} \mathrm{d}x. \tag{6.14}$$

The integrals with $n \neq 0$ in (6.14) can be neglected for $t \ll L_x$, $|x| \leqslant L_x/2$, i.e.

$$J^{(P)} \cong \int_{x-t}^{x} \left[\frac{\partial^2 \Psi^{(L)}}{\partial y \partial T} \right]_{y=0} \mathrm{d}x, \quad t \ll L_x, |x| \leqslant L_x/2. \tag{6.15}$$

However, for larger times $t = O(L_x)$ one should take into account the integral with $n = 1$:

$$J^{(P)} \cong \int_{x-t}^{x} \left[\frac{\partial^2 \Psi^{(L)}}{\partial y \partial T} \right]_{y=0} \mathrm{d}x + \int_{x-t+L_x}^{x+L_x} \left[\frac{\partial^2 \Psi^{(L)}}{\partial y \partial T} \right]_{y=0} \mathrm{d}x, \quad t = O(L_x), |x| \leqslant L_x/2. \tag{6.16}$$

The formulae (6.15), (6.16) are simply interpreted. The second term in (6.12) is the Kelvin wave generated by the periodically localized structure $\tilde{\Psi}_0^{(P)}$. In each periodic

box this wave almost coincides with corresponding compensating jet radiated by the corresponding localized QG motion in the middle of the box up to the time $t \ll t_0 = O(L_x)$. Here t_0 is the time for the compensating jet produced in the box n to reach the localized motion domain in the box $n-1$ located to the right of the box n as it is shown in figure 10.

We now consider the last term in (6.12) related to the along-shore current $\delta\Psi_{B0}\mathrm{e}^{-y}$ providing QG mass conservation. If the period $L_x \leqslant 1/\varepsilon$ then for times $t \ll L_x$ the last term in (6.12) is small,

$$\Psi_{B0} - \varepsilon t \frac{\partial \Psi_{B0}}{\partial T} = O(\delta\varepsilon^2 t^2) \ll \varepsilon O\left(\frac{t^2}{L_x^2}\right) \ll \varepsilon, \tag{6.17}$$

and can be neglected. In the case $L_x \gg 1/\varepsilon$, i.e. $\delta \ll \varepsilon$, this term also can be neglected at $t \ll L_x$. Thus, for any period $L_x \gg 1$ the periodic solution $P^{(P)}$ in each periodic box is closed to the corresponding localized solution $P^{(L)}$ at times $t \ll L_x$.

Thus, our comparison shows that for a fixed period L_x larger than the typical scale L_{loc} of the localized field $\Psi_I^{(L)}$ the interaction between adjacent boxes can be neglected up to time $T_r = O(L_x/c_K)$ where c_K is a Kelvin wave phase speed (equal to 1 in our scaling). This is related to the fact that the motion in a given box m does not depend on the adjacent boxes until the lowest-order Kelvin wave and the compensating jet radiated by the localized perturbation $\Psi_I^{(L)}(x + mL_x, y)$ reach the 'next' perturbation $\Psi_I^{(L)}(x + (m-1)L_x, y)$. At times $t \ll T_r$ the periodic boxes can be approximately considered as isolated ones and the zero boundary condition (1.9) can be used to describe the geostrophic component in each of these boxes. For times $t \geqslant T_r$ the boxes influence each other, and one should take into account the along-wall uniform current $\Psi_B(T)\mathrm{e}^{-y}$ evolving in the slow time T and providing the slow mass conservation in the periodic case. Note that the magnitude of this current is $O(1/L_x)$ and tends to zero with increasing L_x.

The above periodic case is in some sense analogous to the case of a localized perturbation in a closed basin. Our analysis allows us to expect that the geostrophic adjustment in the closed basin develops in the same way as in the periodic case (6.1), i.e. the adjustment is accompanied by the radiation of the lowest-order Kelvin wave and the compensating jet propagating around the basin to the right of the localized perturbation, the signal being exponentially small ahead of the wave and jet. For the wave and jet to reach the location of the initial perturbation from the 'other' side, a time $T_r = O(L_b/c_K)$ is required where L_b is a typical basin size. Obviously, the time T_r increases with increasing basin scale L_b. On times $t \leqslant T_r$ a zero boundary condition such as (1.9) can be used for the geostrophic component, for times $t > T_r$ conditions such as (6.2) should be posed. For 'small' basins with $L_b \leqslant R_d/\varepsilon$ the time $T_r \leqslant 1/f\varepsilon$, and conditions like (6.2) are required to describe the slow geostrophic evolution. For larger basins with $L_b > R_d/\varepsilon$ (for example, in the ocean) a condition such as (1.9) can be used up to times of the order of $T_r > 1/f\varepsilon$ for the localized QG perturbations.

Thus, the approximation of infinite domain can be used if (i) the typical basin scale greatly exceeds the typical size of the localized perturbation and the Rossby scale; (ii) the time does not exceed the typical time T_r which is required for the Kelvin wave to travel the typical basin scale.

Finally, we consider dynamics of the along-wall current $\Psi_B(T)\mathrm{e}^{-y}$. For the periodic motion the total mass of the QG component is conserved in each periodic box; therefore, by virtue of (6.5) the along-wall current $\Psi_B(T)\mathrm{e}^{-y}$ can be considered as a flow compensating variation of mass of the component $\tilde{\Psi}^{(P)}$. One can show that this

current is formed by the periodic forced Kelvin wave generated by the component $\tilde{\Psi}^{(P)}$. This is especially clearly seen for times $t \ll 1/\varepsilon$ when solution (6.12) takes the form

$$P^{(P)} \cong \tilde{\Psi}_0^{(P)}\Big|_{T=0} + \varepsilon t \frac{\partial \tilde{\Psi}_0^{(P)}}{\partial T}\Big|_{T=0} + \varepsilon \mathrm{e}^{-y} \int_{x-t}^{x} \left[\frac{\partial^2 \tilde{\Psi}_0^{(P)}}{\partial y \partial T}\right]_{y=0,T=0} \mathrm{d}x$$

$$= \tilde{\Psi}_0^{(P)}\Big|_{T=0} + \varepsilon t \frac{\partial \tilde{\Psi}_0^{(P)}}{\partial T}\Big|_{T=0} + \varepsilon t \mathrm{e}^{-y} \left\langle \left[\frac{\partial^2 \tilde{\Psi}_0^{(P)}}{\partial y \partial T}\right]_{y=0,T=0} \right\rangle + \varepsilon \mathrm{e}^{-y} s \qquad (6.18)$$

where s is a function periodic in x and bounded in t. The angle brackets denote averaging in x:

$$\langle a \rangle = \frac{1}{L_x} \int_0^{L_x} a \, \mathrm{d}x. \qquad (6.19)$$

It is seen from (6.18) that the propagation of the forced periodic Kelvin wave gives rise to an along-wall current linearly growing in time t (the last term on the right-hand side of (6.18)).This current is approximately described by the streamfunction $\Psi_B(T)\mathrm{e}^{-y}$ at times $t \ll 1/\varepsilon$ with the boundary value $\Psi_B(T)$ corresponding to the linearly growing mass of the forced Kelvin wave.

For larger times an analogous conclusion can be drawn using the equation

$$\frac{\partial \Psi_B}{\partial T} = \frac{\partial}{\partial t} \left\langle \int_{x-t}^{x} \frac{\partial^2 \tilde{\Psi}^{(P)}}{\partial y \partial T}\Big|_{y=0} \mathrm{d}x \right\rangle, \qquad (6.20)$$

which readily follows from (6.7). By virtue of (6.20), the change of mass of the QG along-wall current is exactly equal to the change of mass of the forced Kelvin wave.

7. Summary and conclusion

We have analysed the evolution of a localized flow near a straight infinite boundary when the total mass is not conserved within the equivalent-barotropic quasi-geostrophic (QG) approximation. A simple formula expressing the total geostrophic mass in terms of the QG potential vorticity is derived and used to estimate the range of the geostrophic mass variability. The behaviour of the total mass is analysed for the system of two point vortices interacting with a wall. The evolution of distributed localized perturbations is examined by means of numerical experiments using the QG model. Two types of time variability of the total geostrophic mass are revealed: oscillating (the mass oscillates near some mean value) and limiting (the mass tends to some constant value with increasing times).

The equation relating the geostrophic mass to the QG potential vorticity shows that the total geostrophic mass changes are related to the displacements of fluid particles perpendicular to the boundary $y = 0$; displacements along the boundary do not affect the total mass. This equation written in the Lagrangian variables is used to estimate the range of the geostrophic mass variability. The bounds of the mass are expressed in terms of the initial geostrophic elevation field. If the QG potential vorticity has one sign, then the absolute value of total geostrophic mass is maximal when all fluid particles are located along the straight line $y = \bar{y}_e$ where $\bar{y}_e$ is the distance from the quasi-geostrophic PV centroid to the wall (a conserved quantity).

These formulae for total geostrophic mass and corresponding estimates were generalized to the case of a system of point vortices interacting with the wall and each other. The system of two point vortices was examined in detail. It was shown that if the initial distance between the vortices is sufficiently small then the vortices move periodically, rotating around some moving centre. Correspondingly, the total mass $\overline{M}_2$ and its time derivative $\dot{\overline{M}}_2$ are periodical functions of time, the absolute value of the mass being maximal when the system is elongated along the wall and minimal for the system elongated perpendicular the wall. If the initial distance is sufficiently large, then the motion of the pair is non-periodic, and the distance between the vortices increases monotonically starting from some time. Correspondingly, the interaction between the vortices weakens, and as time passes, the vortices move almost rectilinearly and uniformly along the boundary. With increasing time, the total mass $\overline{M}_2$ tends to a constant value.

Distributed localized perturbations were examined numerically using the QG model. The evolution of the distributed dipole is qualitatively similar to the evolution of a pair of point vortices opposite in sign. Interaction with the boundary results in the destruction of the dipole, and the vortices gradually move apart from each other: eventually the couple splits into two monopoles moving in opposite directions along the boundary. In the course of time, the total mass increases and tends to a new constant value. The change of the mass can exceed 50% of the initial value in this case, i.e. it could become significant.

The evolution of monopolar vortices is qualitatively similar to the behaviour of a pair of vortices of the same sign. The total mass variability in this case is substantially less than for the dipole. The main change of the mass takes place during an initial adaptation period, and later the mass oscillates with small amplitude near some mean value. The mass is minimal (maximal) when the perturbation is elongated perpendicular to (along) the wall, as it is for the point vortex pair.

Considering the next-order dynamics, we found that the conservation of the total mass and circulation is provided by a compensating jet taking away the surplus, or shortage, of mass from the localized lowest-order slow disturbance. A simple representation for the compensating jet was obtained for both oscillating and limiting regimes revealed by the QG analysis. It is seen from this representation that the along-wall jet expands with the fast speed of a Kelvin wave to the right of the initial perturbation. The slow time-dependent amplitude $-\partial\overline{M}/\partial T$ determines the jet sign and intensity at each moment. In the oscillating regime the jet sign and intensity also slowly (in comparison with the jet propagation) oscillate. If the mass $\overline{M}$ tends to a constant value in the course of time, then the jet sign does not change and the jet amplitude slowly tends to zero.

Limits of validity of the model considered when a localized disturbance interacts with an infinitely long boundary are discussed. The approximation of an infinite domain can be used if (i) the typical basin scale greatly exceeds the typical size of the localized perturbation and the Rossby scale; (ii) the time does not exceed the typical time which is required for the Kelvin wave to travel the typical basin scale. These conditions are typical for synoptic eddies of 100 km spatial scale and 10 days temporal scale in the ocean with a basin scale of few thousands km and baroclinic Kelvin wave speed about $2\,\mathrm{m\,s^{-1}}$.

We appreciate useful comments by the associate editor and reviewers. Many thanks to Lisa Cugini for careful editorial assistance. This study was supported by the RFBR Grant # 02-05-64019, the NSF Grant OCE 0220999, and the ONR, Ocean

Science Division. G.S. appreciates support and hospitality of the Department of Mathematical Sciences of Loughborough University during Visiting Professorship funded by the Liverhulme Trust F00261L.

Appendix A

According to the Lagrange multipliers method, the following functional is introduced:

$$N = -\int_{y_0>0} Q_0(x_0, y_0)[1 - \lambda\bar{y} - \mathrm{e}^{-\bar{y}}]\,\mathrm{d}x_0\,\mathrm{d}y_0 \tag{A 1}$$

where λ is a Lagrange multiplier. The corresponding Euler equation for the extremal $\bar{y} = \bar{y}_e(x_0, y_0)$ is written in the form

$$\lambda - \mathrm{e}^{-\bar{y}_e} = 0, \tag{A 2}$$

whence it follows that $\bar{y}_e$ is a constant related to λ by the equation

$$\bar{y}_e = \ln\lambda. \tag{A 3}$$

The constants $\bar{y}_e$ and λ are determined from equation (2.13*b*),

$$\bar{y}_e = \frac{\displaystyle\int_{y_0>0} y_0 Q_0(x_0, y_0)\,\mathrm{d}x_0\,\mathrm{d}y_0}{\displaystyle\int_{y_0>0} Q_0(x_0, y_0)\,\mathrm{d}x_0\,\mathrm{d}y_0}, \tag{A 4}$$

and (A 2).

The second variation of the functional N on the extremal $\bar{y} = \bar{y}_e$ is equal to

$$\delta^2 N = -\frac{\alpha^2}{2}\mathrm{e}^{-\bar{y}_e}\int_{y_0>0} \eta^2 Q_0(x_0, y_0)\,\mathrm{d}x_0\,\mathrm{d}y_0. \tag{A 5}$$

Here $\alpha\eta$ is a perturbation to $\bar{y}_e$ such that η is an arbitrary bounded function and $\alpha \to 0$. Obviously, $\delta^2 N$ is sign-definite only if the PV Q_0 does not change its sign, i.e. the sufficient conditions for existence of a maximum or minimum of the functional $\overline{M_a}$ are satisfied only in the case of PV of fixed sign. Also, the coordinate $\bar{y}_e$ is positive for Q_0 of a fixed sign. Thus, for Q_0 of a fixed sign the absolute value of functional (2.13*a*) is maximal on the extremal $\bar{y} = \bar{y}_e$.

Appendix B

B.1. *Behaviour of $\Psi^{(L)}$ at infinity*

Let us write equations (1.4*d*), (1.5), and (1.9) for $\Psi^{(L)}$ in the form

$$\nabla^2\frac{\partial\Psi^{(L)}}{\partial T} - \frac{\partial\Psi^{(L)}}{\partial T} = -J\left(\Psi^{(L)}, \nabla^2\Psi^{(L)}\right), \quad \Psi^{(L)}\big|_{T=0} = \Psi_I^{(L)}(x, y), \tag{B 1a, b}$$

$$\Psi^{(L)} = 0 \text{ at } y = 0. \tag{B 1c}$$

At some moment $T = T_0$ the field $\Psi^{(L)}$ is strongly localized, so that

$$\Psi^{(L)} = O(\mathrm{e}^{-r}), r = \sqrt{x^2 + y^2} \to \infty. \tag{B 2}$$

By virtue of (B 1*a*, *c*) the same estimate is valid for the time derivative $\partial\Psi^{(L)}/\partial T$:

$$\frac{\partial\Psi^{(L)}}{\partial T} = O(\mathrm{e}^{-r}), \ r \to \infty. \tag{B 3}$$

It follows from (B 2), (B 3) that the estimate (B 2) is valid at the next moment $T = T_0 + \mathrm{d}T$, i.e. all time. Thus if the initial field $\Psi_I^{(L)}$ is $O(\mathrm{e}^{-r})$ then this estimate remains unchanged in time.

B.2. *Behaviour of* $\partial\Psi_B/\partial T$ *at* $T = 0$

Let us write (1.4*d*) for $\Psi^{(P)}$ in the form analogous (B1*a*):

$$\nabla^2\frac{\partial\Psi^{(P)}}{\partial T} - \frac{\partial\Psi^{(P)}}{\partial T} = -J\left(\Psi^{(P)}, \nabla^2\Psi^{(P)}\right), \tag{B 4}$$

and integrate (B 4) in x from 0 to L_x. As a result we obtain

$$s_{yy} - s = -\int_0^{L_x} J\left(\Psi^{(P)}, \nabla^2\Psi^{(P)}\right)\mathrm{d}x, \quad s = \int_0^{L_x}\frac{\partial\Psi^{(P)}}{\partial T}\,\mathrm{d}x. \tag{B 5a, b}$$

We now multiply (B 5*a*) by e^{-y} and integrate the resulting equation in y from 0 to ∞; using boundary conditions (6.2) we have

$$\frac{\partial\Psi_B}{\partial T} = \frac{1}{L_x}\int_0^\infty \mathrm{e}^{-y}\,\mathrm{d}y\int_0^{L_x}\frac{\partial\Psi^{(P)}}{\partial x}\frac{\partial^2\Psi^{(P)}}{\partial y^2}\,\mathrm{d}x. \tag{B 6}$$

Correspondingly, at the initial moment

$$\left.\frac{\partial\Psi_B}{\partial T}\right|_{T=0} = \frac{1}{L_x}\int_0^\infty \mathrm{e}^{-y}\,\mathrm{d}y\int_0^{L_x}\frac{\partial\Psi_I^{(P)}}{\partial x}\frac{\partial^2\Psi_I^{(P)}}{\partial y^2}\,\mathrm{d}x. \tag{B 7}$$

By virtue of initial condition (6.1) we have to within exponentially small values

$$\frac{\partial\Psi_I^{(P)}}{\partial x}\frac{\partial^2\Psi_I^{(P)}}{\partial y^2} = \sum_{-\infty}^{\infty} g(x + nL_x, y), \;\; g(x, y) = \frac{\partial\Psi_I^{(L)}}{\partial x}\frac{\partial^2\Psi_I^{(L)}}{\partial y^2}. \tag{B 8a, b}$$

It readily follows from (B 7), (B 8) that

$$\left.\frac{\partial\Psi_B}{\partial T}\right|_{T=0} = \frac{1}{L_x}\int_0^\infty \mathrm{e}^{-y}\,\mathrm{d}y\int_{-\infty}^{\infty}\frac{\partial\Psi_I^{(L)}}{\partial x}\frac{\partial^2\Psi_I^{(L)}}{\partial y^2}\,\mathrm{d}x = O\left(\frac{1}{L_x}\right).$$

Appendix C

The localized solution to the equation $\nabla^2\Psi - \Psi = Q$ obeying the no-flux condition (1.9) is written as follows:

$$\Psi(x, y, t) = -\frac{1}{2\pi}\int_{y'>0} Q(x', y', t)[K_0(r) - K_0(\bar{r})]\,\mathrm{d}x'\,\mathrm{d}y', \tag{C 1a}$$

where

$$r = \sqrt{(x - x')^2 + (y - y')^2}, \quad \bar{r} = \sqrt{(x - x')^2 + (y + y')^2} \tag{C 1b}$$

and $K_n(z), n = 0, 1, \ldots$ denotes the nth-order modified Bessel function. Inside the integrand in (C 1*a*) the terms proportional to $K_0(r)$ and $K_0(\bar{r})$ correspond to the contribution made by the 'real' and 'image' point vortices, respectively.

We now consider a system of point vortices interacting with each other and with their images and moving along some trajectories $\boldsymbol{r} = \boldsymbol{r}_k(t)$. Here $\boldsymbol{r} = \boldsymbol{r}(x, y)$ and $k = 1, 2, \ldots N$ denote the radius vector and the number of the vortex, respectively. The streamfuction Ψ obeys the equations:

$$\nabla^2\Psi - \Psi = \sum_{k=1}^{N} A_k\delta(x - x_k(t))\delta(y - y_k(t)), \; \Psi|_{y=0} = 0 \tag{C 2a, b}$$

where A_k is a constant amplitude of kth point vortex and $\delta(z)$ is the Dirac delta-function. The solution to (C2) is written in the form

$$\Psi = \frac{1}{2\pi}\sum_k A_k[K_0(|\boldsymbol{r}-\boldsymbol{r}_k|) - K_0(|\boldsymbol{r}-\bar{\boldsymbol{r}}_k|)], \quad \boldsymbol{r}_k = (x_k, y_k), \quad \bar{\boldsymbol{r}}_k = (x_k, -y_k). \tag{C 3a, b}$$

In (C 3) the radius vectors $\boldsymbol{r}_k$ and $\bar{\boldsymbol{r}}_k$ correspond to the 'real' and 'image' vortices, respectively.

The motion of the nth vortex is due to its interaction with its own image and with other vortices and their images. Equations describing this motion are obtained in the usual way and can be written in the form

$$\dot{x}_n = \frac{A_n}{2\pi}K_1(2y_n) + \frac{1}{2\pi}\sum_{k\neq n} A_k\left[\frac{\bar{y}_{nk}K_1(\bar{r}_{nk})}{\bar{r}_{nk}} - \frac{y_{nk}K_1(r_{nk})}{r_{nk}}\right], \tag{C 4a}$$

$$\dot{y}_n = \frac{1}{2\pi}\sum_{k\neq n} A_k x_{nk}\left[\frac{K_1(r_{nk})}{r_{nk}} - \frac{K_1(\bar{r}_{nk})}{\bar{r}_{nk}}\right], \tag{C 4b}$$

where

$$r_{nk} = \sqrt{(x_n-x_k)^2+(y_n-y_k)^2}, \quad x_{nk} = x_n - x_k, \quad y_{nk} = y_n - y_k, \tag{C 4c}$$

$$\bar{r}_{nk} = \sqrt{(x_n-x_k)^2+(y_n+y_k)^2}, \; \bar{y}_{nk} = y_n + y_k. \tag{C 4d}$$

The first term on the right-hand side of (C 4a) describes an effect on the vortex of its own image; clearly, this effect initiated the displacement of the vortex along the boundary.

Multiplying (C 4b) by A_n and summing over n from 1 to N we arrive at an analogue of integral (2.11) for the system of point vortices

$$\sum_n A_n y_n = \text{const.} \tag{C 5}$$

Integrating Ψ in (C3) over the plane $y > 0$, using the formula

$$\int_{-\infty}^{\infty} K_0(\sqrt{x^2+y^2})\,\mathrm{d}x = \pi \mathrm{e}^{-|y|}$$

when deriving (C 6) (Gradshtein & Ryzhik 1980), we obtain the total mass of the system of N point vortices (cf. analogous formula (2.6) for the distributed fields):

$$\overline{M}_N = -\sum_k A_k(1-\mathrm{e}^{-y_k}). \tag{C 6}$$

One can derive an estimate analogous to (2.15) using the Lagrange multipliers method to analyse the extrema of the function

$$\overline{M}_N^{(a)} = \overline{M}_N^{(a)}(y_1, y_2, \ldots y_N) = -\sum_k A_k(1-\mathrm{e}^{-y_k}) \tag{C 7}$$

under condition (C 5) given the amplitudes A_k. The analysis shows that if the A_k are of the same sign then the modulus $|\overline{M}_N^{(a)}|$ has a maximum equal to

$$\left|\overline{M}_N^{(a)}\right|_{\max} = (1-\mathrm{e}^{-y_c})\sum_k |A_k| \tag{C 8}$$

at the point

$$y_1 = y_2 = \cdots = y_N = y_c = \sum_k A_k y_k \Big/ \sum_k A_k. \tag{C 9}$$

Respectively, estimate (2.15) in the case of a system of N point vortices is rewritten as

$$|\overline{M}_N| \leqslant \left|\overline{M}_N^{(a)}\right|_{\max} = (1 - \mathrm{e}^{-y_c}) \sum_k |A_k|. \tag{C 10}$$

Using (C 4*b*) one can derive the following useful formula for the mass time derivative:

$$\dot{\overline{M}}_N = -\frac{1}{4\pi} \sum_{k \neq n} A_k A_n x_{nk} \left[\frac{K_1(r_{nk})}{r_{nk}} - \frac{K_1(\bar{r}_{nk})}{\bar{r}_{nk}} \right] (\mathrm{e}^{-y_n} - \mathrm{e}^{-y_k}). \tag{C 11}$$

REFERENCES

Dorofeyev, V. L. & Larichev, V. D. 1992 The exchange of fluid mass between quasi-geostrophic and ageostrophic motions during the reflection of Rossby waves from a coast. 1. The case of an infinite rectilinear coast, *Dyn. Atmos. Oceans* **16**, 305–329.

Fedorov, A. V. & Melville, W. K. 1996 Hydrauvlic jumps at boundaries in rotating fluids. *J. Fluid Mech.* **324**, 55–82.

Gill, A. E. 1976 Adjustment under gravity in a rotating channel. *J. Fluid Mech.* **77**, 603–621.

Gradshteyn, I. S. & Ryzhik, I. M. 1980 *Table of Integrals, Series, and Products*. 2nd Edn. Academic.

Grimshaw, R. & Allen, J. 1988 Low-frequency baroclinic waves off coastal boundaries. *J. Phys. Oceanogr.* **18**, 1124–1143.

Helfrich, K. R., Kuo, A. C. & Pratt, L. C. 1999 Nonlinear Rossby adjustment in a channel. *J. Fluid Mech.* **390**, 187–222.

Helfrich, K. R. & Pedlosky, J. 1995 Large-amplitude coherent anomalies in baroclinic zonal flows. *J. Atmos. Sci.* **52**, 1615–1629.

Hermann, A. J., Rhines, P. & Johnson, E. R. 1989 Nonlinear Rossby adjustment in a channel: beyond Kelvin waves. *J. Fluid Mech.* **205**, 469–502.

Kamenkovich, V. M. & Reznik, G. M. 1978 Rossby waves. In *Physics of the Ocean. V.2. Hydrodynamics of the Ocean*, pp. 300–358. Moscow (in Russian).

McCalpin, J. D. 1995 Rossby wave generation by poleward propagating Kelvin waves: The midlatitude quasigeostrophic approximation. *J. Phys. Oceanogr.* **25**, 1415–1425.

McWilliams, J. C. 1977 A note on a consistent quasigeostrophic model in a multiply connected domain. *Dyn. Atmos. Oceans* **1**, 427–441.

Miles, J. W. 1972 Kelvin waves on oceanic boundaries. *J. Fluid Mech.* **55**, 113–127.

Pedlosky, J. 1987 *Geophysical Fluid Dynamics*. Springer.

Phillips, N. A. 1954 Energy transformations and meridional circulations associated with simple baroclinic waves in a two-level, quasi-geostrophic model. *Tellus* **6**, 273–286.

Reznik, G. M. & Grimshaw, R. 2002 Nonlinear geostrophic adjustment in the presence of a boundary. *J. Fluid Mech.* **471**, 257–283 (referred to herein as RG).

Reznik, G. M. Zeitlin, V. & Ben Jelloul, M. 2001 Nonlinear theory of geostrophic adjustment. Part 1. Rotating shallow-water model. *J. Fluid Mech.* **445**, 93–120.

Tomasson, G. G. & Melville, W. K. 1992 Geostrophic adjustment in a channel: nonlinear and dispersive effects. *J. Fluid Mech.* **241**, 23–58.